PERGAMON

International Journal of Multiphase Flow 28 (2002) 963–996

International Journal of Multiphase Flow

www.elsevier.com/locate/ijmulflow

Laminar stratified pipe flow

T.S. Ng, C.J. Lawrence *, G.F. Hewitt

Department of Chemical Engineering & Chemical Technology, Imperial College of Science, Technology and Medicine, Prince Consort Road, London SW7 2BY, UK

Received 15 February 2001; received in revised form 16 December 2001

Abstract

The Boundary Element Method (BEM) has been used to evaluate the integral and local flow properties of two-phase laminar–laminar stratified flow in a pipe for interface shapes determined by exact solution of the Young–Laplace equation. Results are presented for the volumetric flow rates, the interface and wall shear stresses and the velocity profiles on the interface and through the cross-section of the pipe.

For the case of a flat planar interface, the results obtained from the BEM were compared against those from the analytical solution for a 50% holdup (i.e. with a flat interface passing through the horizontal axis) and with previous numerical solutions obtained using the bipolar coordinate system. Comparisons for the case of a circular interface were made with the Fourier integral method described by others. The solutions from the boundary integral method agree very well with these published results for special cases.

Solutions are presented for a range of parameter values. The interface shape is determined by the Bond number, holdup or contact angle. The flow is controlled by these parameters, as well as the viscosity ratio, and the pipe inclination, which determines the relative driving forces on the two fluids.

It is concluded that the BEM offers great flexibility and accuracy in addressing this class of flows.

Keywords: Laminar–laminar flow; Exact interface shape; Boundary Element Method

1. Introduction

In stratified two phase flow in a pipe, the two phases flow in separate regions with the lighter fluid flowing in the upper part of the pipe. The most important case for technological applications is flow in a pipe of circular cross-section. The interface separating the two flow regions is often assumed to be planar, but in the general case, it has a curved form, the shape being determined by the contact angle at the pipe wall and a balance between gravitational and surface tension forces.

* Corresponding author. Tel.: +44-20-759-45622; fax: +44-20-759-45700.
E-mail address: cjl@ic.ac.uk (C.J. Lawrence).

0301-9322/02/$ - see front matter
PII: S0301-9322(02)00004-6

Stratified two-phase flow has been of long-standing interest from both the practical and the theoretical points of view. Many pipeline systems are designed to operate in the stratified flow region; stratified flow gives lower pressure gradients than slug flow and does not suffer from the problems of intermittent behaviour that slug flow produces. In many practical stratified flows, one or both phases may be turbulent (particularly in gas–liquid flows) and partial mixing (inter-entrainment) of the phases may occur at high velocities, but solution of the flow field for the case where both flows are laminar and where the interface is undisturbed still represents an important base case from which much can be learned. This laminar–laminar flow case is also reasonably common in some practical applications in viscous liquid–liquid flow systems. Thus, there have been a variety of studies of this case for both horizontal and inclined pipelines.

Due to the complex flow geometry of stratified flow in circular conduits, most studies have used either 'equivalent' models of flow between parallel plates or an averaged two-fluid formulation assuming a planar interface between the phases. However, the accuracy of such averaged models in predicting the integral flow characteristics, such as the axial pressure drop and the in situ holdup is hard to quantify and sometimes poor. A more satisfactory approach is to obtain the velocity profiles, stress distributions and other local flow properties from a more rigorous treatment of the two-dimensional Navier–Stokes equation. These solutions can then be used as a basis for determining the integral quantities. Several researchers have obtained analytical and numerical solutions to such problems for various assumed interface geometries and have proposed mechanistic methods to determine the local and integral flow properties.

Rusell and Charles (1959) examined two different flow systems for two immiscible, incompressible Newtonian fluids in laminar stratified flow, between parallel plates, and with the two liquids flowing concentrically in a circular pipe. The positions of the interface corresponding to a minimum in the pressure drop or the power requirement were determined for specific systems. It was concluded that the maximum reduction in power obtained in the pipe system with concentric flow was considerably greater than that in the parallel plate system. This was due to the reduction of shear when the less viscous phase flows next to the pipe wall.

Exact analytical solutions can be obtained for special interface geometries in a circular pipe. By assuming a planar interface to be situated in the horizontal diametrical plane, with a holdup of 50%, Yu and Sparrow (1967) derived an exact solution by coupling a suitable Green's function with their reduced velocity equations. Brauner et al. (1996) carried this solution further and obtained the variation of the wall shear stress, and its discontinuity across the interface, for this unique flow scenario. Packham and Shail (1971), obtained the exact solution for a co-current flow in a duct with a flat planar diametrical interface. They showed that when the cross-section was symmetrical with respect to the interface, the solution could be expressed in terms of two separate solutions corresponding to the flow of a single liquid in the whole pipe and in a half pipe bounded by the interface. Kurban (1997) also reported an exact solution to the same problem obtained by expressing the solution of the Navier–Stokes equations as a sum of the particular and Laplace solutions. The particular solution was determined by suitable expressions that satisfied the boundary and interface conditions, and a Fourier series solution was obtained for the Laplace equations. Wall and interfacial shear stresses, together with the phase flow rates were also obtained.

Gemmell and Epstein (1962) compared experimental data and numerical solutions for co-current laminar stratified flow in a circular pipe for various viscosity ratios with a flat fluid–fluid interface at eight different positions. A two-dimensional finite element method was applied with

Cartesian coordinates superimposed onto the circular pipe. They obtained the volumetric flow rate by summing the products of the nodal velocities and the areas of the finite elements. Though not all of the experimental cases appeared to be sharply stratified (in some cases, the interface was wavy), good agreement was obtained for both the in situ holdup and the pressure gradient when both fluids were in laminar flow. The experimental and computed results began to deviate when the less viscous phase (water) entered the transitional and turbulent regions.

Bentwich (1964) derived analytical expressions for the velocity distributions which would hold for all possible annular, lunar and stratified flow configurations with a circular interface. He developed Fourier series and Fourier transform solutions using a bipolar coordinate system. With the motivation of reducing energy requirement for transporting viscous liquids in pipelines by the addition of a less viscous liquid, Bentwich (1976) later proposed an analytical approximation for determining the geometry of the interface of two immiscible liquids, taking into account the interfacial tension, capillary forces and gravity. The two-phase Poiseuille flow problem was then solved by applying an equivalent variational principal with the Rayleigh–Ritz method, in order to obtain the axial velocities and flow rates of the liquids. Here, the solution was approximated using a finite number of functions to represent each velocity field.

Yu and Sparrow (1967) determined closed form solutions for two-component stratified laminar flow in horizontal ducts of arbitrary cross-section. Again, a flat interface was assumed. From the transformation of the momentum equations, the reduced velocity field was expressed as a series of harmonic functions, in the coordinates of a cross-sectional plane, $(x + \mathrm{i}y)^n$. The coefficients in the series for the reduced velocities were determined by the application of the least squares method to satisfy the boundary conditions. The velocities were then integrated to obtain both the volumetric flow rate and the pressure gradient. However, neither the interfacial nor wall shear stresses were calculated.

Ranger and Davis (1979) obtained an explicit analytical solution for the flow of two fluids of different viscosities with a flat interface. They expressed the fluid velocities in terms of Fourier integrals, which were then used to express the volumetric fluxes of each fluid as a single integral. The results agreed well with the numerical solution of Gemmell and Epstein (1962).

A numerical method for solving the physical flow problem of laminar–laminar stratified flow with a plane interface was proposed by Hall (1992). The numerical domain was bounded externally at the pipe walls, with a horizontal grid line across the pipe, coinciding with the interface. The bipolar coordinate system was applied to match this geometry. This coordinate system has advantages for generating a simple grid that fits both the pipe walls and the interface, enabling the boundary conditions to be applied at exact grid locations. A finite volume discretisation method was used, and the solution was obtained via the Tri-Diagonal Matrix Algorithm and the Gauss–Seidel method. Hall and Hewitt (1993) presented comparisons of numerical solutions with those obtained from the integral two-fluid model in order to evaluate the accuracy of the latter.

Brauner et al. (1996) obtained analytical solutions for the local flow properties of flow systems with either a flat or circular arc interface. Both Fourier series and Fourier integral solutions were presented. The coefficients of the Fourier series are independent of the holdup and the viscosity ratio and thus can be determined with ease once the interface curvature is specified. Hence the dimensionless velocity profiles for the whole range of in situ holdups and viscosity ratios could be calculated. Although the number of terms in the Fourier series determined the convergence of the solution, the accuracy of the values obtained for the interfacial velocities and shear stresses

deteriorated near the pipe wall even when the number of terms was increased. The Fourier integral method was more complicated to apply, as the calculation of the spectral functions must be iterated for each specific holdup and viscosity ratio. However, this method provided flow characteristics in the entire domain, including the two contact points at the pipe wall, which were excluded in the solution obtained by Fourier series. Apart from the problem in the vicinity of the contact points at the walls, both solutions yielded practically the same results. Nevertheless, when the variation of the local flow characteristics over the entire interface is of importance, Fourier integrals must be employed. The wall shear stress showed a large variation in the vicinity of the fluid–fluid interface and was discontinuous across the interface. The results provide a better understanding of the hydrodynamic behaviour in the flow field and around the interface.

Moalem Maron et al. (1995) presented data using the Fourier integral calculation procedure for circular arc interfaces, illustrating the effect of interface curvature and in situ holdup on the flow rate ratios. They concluded that the characteristics of the wall shear stress profile in the vicinity of the interface could be used to generalise the definition of thin fluid layers in stratified flows with curved interfaces. These definitions could be different from those based on the in situ holdup criterion. Since stratified two-phase flow represents a basic flow pattern for exploring the transition to other flow patterns, they suggested that their solution for the curved interface could be used as a new basis for stability analyses of stratified layers accounting for the interfacial tension and wall adhesion forces.

Biberg and Halvorsen (2000) obtained detailed solutions for the wall and interfacial shear stresses in pressure driven two-phase laminar stratified pipe flow with a flat interface in terms of Fourier integrals. The solution was written as a linear combination of a single-phase free surface flow term, and a second term that links the phases together and represents the shear driven flow.

Many simplified mechanistic models have been discussed. Brauner et al. (1998) developed the two-fluid model for circular arc interfaces by taking the momentum equations and expressing them in terms of the phase distribution angle and the interface curvature. They compared the solution from the two-fluid model with the corresponding exact solutions in the laminar flow regime over a wide range of interface curvatures and phase flow rates. The two-fluid model tended to over-predict the pressure drop, but it predicted the in situ holdup reasonably well.

All the previous work cited above has been based on approximate forms of the interface geometry. The interface has been represented as perfectly flat or as a circular arc. The exact interface shape for laminar–laminar stratified flow in a circular pipe has recently been determined by Gorelik and Brauner (1999) and Ng et al. (1999b, 2001). Three dimensionless parameters are used to determine the shape of the interface as a solution of the Young–Laplace equation. These are the contact angle at the three-phase line, θ, the holdup of the denser phase, ε, and the Bond number, Bo. The contact angle, θ, is the angle between the interface and the pipe wall, measured through the denser phase; the holdup, ε, is defined as the fraction of the pipe cross-section occupied by the denser fluid; and the Bond number, Bo, is the ratio of gravitational to surface tension forces, defined as

$$Bo = \frac{\Delta\rho g a^2}{\gamma_{AB}} \tag{1}$$

where $\Delta\rho$ is the density difference between the two fluids, g is the gravitational constant, a is the radius of the pipe and γ_{AB} is the interfacial tension.

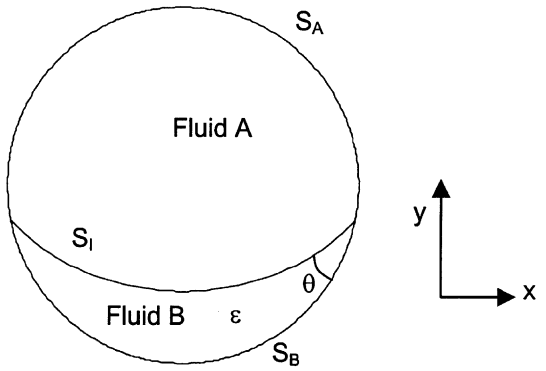

Fig. 1. Schematic diagram of the pipe cross-section, highlighting the parameters used.

Fig. 1 shows the general configuration of the fluids, illustrating the contact angle and holdup. The lighter phase is labelled fluid A (above), and the denser phase is fluid B (below). The flows are assumed to be at steady state, fully developed, and therefore unidirectional.

The aim of the work described here is to present a precise calculation method for two-phase laminar–laminar stratified flows where the interface shape is specified exactly (Ng et al., 2001), and is neither flat nor circular. In the Boundary Element Method (BEM), only the boundary of the region is discretised. The equations governing the problem are converted to integral equations in terms of the unknown function over the boundary of the problem domain. The principal advantage of the BEM over domain type analyses such as the finite element and finite difference methods is that computational time and storage are greatly reduced. (Brebbia, 1978; Stakgold, 1979; Pozrikidis, 1992; El-Zafrany, 1993; Banerjee, 1994). Only values at the boundaries are required to determine flow properties such as the flow rates, interfacial velocities, and the wall and interfacial shear stresses.

Stratified flows are subject to many kinds of instability, which lead to the generation of waves on the interface, or even slugs. Transition from laminar to turbulent flow is also a possibility. Such phenomena are beyond the scope of the present work. However, the present work provides a detailed solution procedure for smooth parallel flow, which could be used as the starting point for a study of instabilities and transitions to other flow regimes.

The underlying mathematical formulation is discussed in Section 2, with the question of convergence being addressed in Section 3. Section 3 also presents comparisons with previous solutions. The results determined from the calculations are presented in Section 4 and the conclusions drawn are summarised in Section 5.

2. Mathematical formulation

2.1. Preliminaries

The dimensionless equations for the axial velocity in phases A and B shown in Fig. 1 are Poisson equations, which can be derived from the Navier–Stokes Equation (Packham and Shail, 1971):

$$\nabla^2 u_{z\mathrm{A}} = -\frac{1}{m}\chi \tag{2}$$

$$\nabla^2 u_{z\mathrm{B}} = -1 \tag{3}$$

where $u_{z\mathrm{A}}$ and $u_{z\mathrm{B}}$ are the local axial velocities of phase A and phase B respectively, and m and χ are dimensionless parameters of the flow problem. Here, m is the viscosity ratio

$$m = \frac{\mu_{\mathrm{A}}}{\mu_{\mathrm{B}}} \tag{4}$$

where μ_{A} and μ_{B} are the viscosities of the two fluids. The dimensionless driving ratio χ is given by

$$\chi = \frac{(-G - \rho_{\mathrm{A}} g \sin\alpha)}{(-G - \rho_{\mathrm{B}} g \sin\alpha)} \tag{5}$$

where ρ is the density of the fluid, g is the gravitational constant and α is the inclination of the pipe (positive for upwards inclined flow). When the pipe is horizontal, α is zero and the dimensionless driving ratio, χ, is unity. G is the axial pressure gradient along the pipe, taken to be negative.

The equations have been made dimensionless using the pipe radius R for the length scale and a velocity scale U chosen as

$$U = \frac{(-G - \rho_{\mathrm{B}} g \sin\alpha) R^2}{\mu_{\mathrm{B}}} \tag{6}$$

Note that U is generally taken to be positive, but it can take negative values as discussed later.

The interface shape is determined by a balance of hydrostatic and surface tension effects, expressed by the Young–Laplace equation. The general solution for the position of the interface (x, y) in a pipe of unit radius is given by Ng et al. (2001) in the parametric form

$$x = \pm\frac{1}{\sqrt{Bo\, b}}\left[-E\left(\frac{\varphi}{2}, -4b\right) + (1+2b)F\left(\frac{\varphi}{2}, -4b\right)\right] \tag{7}$$

and

$$y = \pm\frac{1}{\sqrt{Bo\, b}}\left[-1 + \sqrt{1 + 2b - 2b\cos\varphi}\right] \tag{8}$$

with φ being the parameter of the interface, defined as the angle between the tangent to the interface and the horizontal in the positive x-direction. F and E represent the elliptic integrals of the first and second kind respectively. The Bond number represents the ratio of gravitational and interface forces, and is defined in Eq. (1) above. b is a modified Bond number, based on the (unknown) reference curvature at the centre of the interface, κ_0,

$$b = \frac{Bo}{\kappa_0^2} \tag{9}$$

The appropriate solution for a given case is obtained by imposing the constraint of a particular holdup, ε, and contact angle, θ, to determine κ_0, b and the range of φ in the solution. Sample solutions are given in Fig. 2(a) for a contact angle, $\theta = \pi/3$, Bond number, $Bo = 10$, and various values of the holdup, ε, and in Fig. 2(b) for holdup, $\varepsilon = 0.3$, Bond number, $Bo = 10$, and various values of the contact angle, θ. The reference configuration, $\varepsilon = 0.3$, $Bo = 10$, $\theta = \pi/3$, is used to

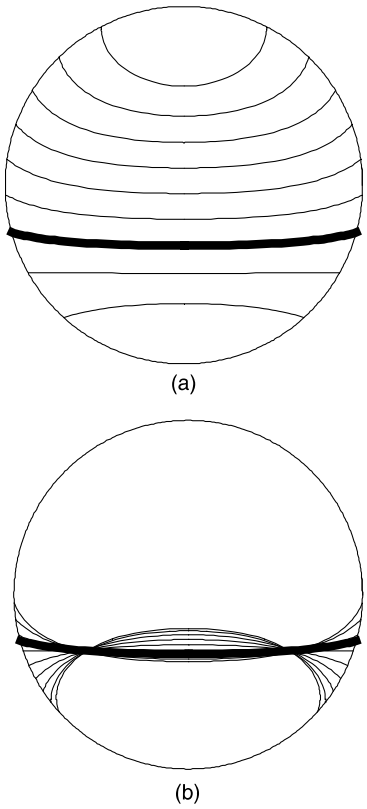

Fig. 2. Exact interface shapes compared to the reference configuration ($\theta = \pi/3$, $Bo = 10$, $\varepsilon = 0.3$): (a) different holdups, $\varepsilon = 0.1, 0.2, \ldots, 0.9$ and (b) different contact angles, $\theta = 0.1\pi, 0.2\pi, \ldots, 0.9\pi$.

assess the affects of the various parameters as discussed below. A catalogue of solutions has been presented by Ng et al. (2001) for the full range of parameters.

The stratified laminar flow problem is characterised by five dimensionless parameters, namely, the holdup, ε, the contact angle, θ, the Bond number, Bo, the viscosity ratio, m and the dimensionless driving ratio, χ. For oil (Shell Tellus 22)–water flows in 1.5 in. pipelines, typical values for the contact angle, Bond number and viscosity ratio are 0.3π, 10 and 45, respectively. These are used for the reference configuration, together with a representative value of holdup, $\varepsilon = 0.3$, and the driving ratio for a horizontal pipe, $\chi = 1$. The numerical solution presented here determines the phase flow rates for given values of the pressure gradient and the holdup. The more practical problem of evaluating the pressure gradient and the phase holdup for given values of the volumetric flow rates can be solved by iterative use of the method presented here.

2.2. Particular solution

Particular solutions are chosen to satisfy the no-slip condition on the wall, and the velocities are written in the form:

$$u_{z\mathrm{A}} = \frac{\chi}{4m}(1 - r^2) + f_{\mathrm{A}} \tag{10}$$

$$u_{z\mathrm{B}} = \frac{1}{4}(1 - r^2) + f_{\mathrm{B}} \tag{11}$$

where r is the dimensionless radial coordinate which is zero at the pipe centreline and unity at the pipe wall. f is the difference between the true velocity, u_Z, and the particular solution (i.e. f is the homogenous solution).

Eqs. (2) and (3) are transformed into Laplace equations for f where

$$\nabla^2 f_{\mathrm{A}} = 0 \tag{12}$$

$$\nabla^2 f_{\mathrm{B}} = 0 \tag{13}$$

The no slip conditions at the walls, S_{A} and S_{B}, then give Dirichlet conditions

$$f_{\mathrm{A}} = 0$$

$$f_{\mathrm{B}} = 0$$

The continuity of velocity and shear stress on the fluid–fluid interface, S_{I}, require that

$$f_{\mathrm{A}} - f_{\mathrm{B}} = \frac{m - \chi}{4m}(1 - r^2) \tag{14}$$

$$m(\underline{n} \cdot \nabla f_{\mathrm{A}}) - \underline{n} \cdot \nabla f_{\mathrm{b}} = \frac{\chi - 1}{2}\underline{n} \cdot \underline{x} \tag{15}$$

where $\underline{x}$ is the (dimensionless) position vector with respect to the origin at the centre of the pipe, and $\underline{n}$ is the unit normal on the interface, directed into the lower phase B.

The system of equations (12) to (15) is linear in χ, so the solution at any value of χ can be obtained via interpolation (or extrapolation) between solutions at any two values, say $\chi = 0$ and $\chi = 1$. Hence,

$$f_\chi = f_0 + \chi(f_1 - f_0) \tag{16}$$

where f_a is the solution at $\chi = a$.

2.3. The boundary integral equation

In the solution of the Laplace equations, a Green's function is introduced which satisfies the condition at the pipe wall,

$$G(\underline{x}, \underline{x}_0) = \frac{1}{2\pi} \ln\left(\frac{|\underline{x} - \underline{x}_0|}{|\underline{x}_0||\underline{x} - \hat{\underline{x}}_0|}\right) \tag{17}$$

where $\underline{x}$ is the field point, $\underline{x}_0$ is the source point, and $\hat{\underline{x}}_0 = \underline{x}_0/|\underline{x}_0|^2$ is the image point of $\underline{x}_0$.

The boundary integral equation is derived from Green's Theorem for two scalar fields f and g on a domain A with boundary S.

$$\int\int_A (f\nabla^2 g - g\nabla^2 f)\,\mathrm{d}A = \int_S (f\underline{n} \cdot \nabla g - g\underline{n} \cdot \nabla f)\,\mathrm{d}S \tag{18}$$

where $\underline{n} \cdot \nabla g$ is the derivative of the scalar field g in the direction of the outward normal vector $\underline{n}$ on the boundary S of region A.

Now, f is made the solution of the problem; and g is replaced by the Green's function. Upon substitution and simplification, equations relating the value of f at the field point $\underline{x}_0$ to the values at points $\underline{x}$ on the interface are obtained.

$$f_A(\underline{x}_0) = \int_{S_I} (f_A(\underline{x})\underline{n}(\underline{x}) \cdot \nabla G(\underline{x}, \underline{x}_0) - G(\underline{x}, \underline{x}_0)\underline{n}(\underline{x}) \cdot \nabla f_A(\underline{x}))\, dS(\underline{x}) \tag{19}$$

$$f_B(\underline{x}_0) = -\int_{S_I} (f_B(\underline{x})\underline{n}(\underline{x}) \cdot \nabla G(\underline{x}, \underline{x}_0) - G(\underline{x}, \underline{x}_0)\underline{n}(\underline{x}) \cdot \nabla f_B(\underline{x}))\, dS(\underline{x}) \tag{20}$$

where the negative sign in Eq. (20) arises because the normal on the interface has been chosen to point outwards for phase A and hence, *inwards* for phase B. The gradient operator acts on the first argument, $\underline{x}$, of G. Here S_I denotes the liquid–liquid interface. Integrals around the pipe wall are not required because of the choice of G in Eq. (17).

The area inside region A and within a very small distance of any point $\underline{x}_i$ which lies on the boundary, S, is half that for a point $\underline{x}_0$ which lies within area A. Hence, if $\underline{x}_0$ is replaced by $\underline{x}_i$, a factor of 0.5 will be included on the left-hand side of Eqs. (19) and (20). On the right-hand side, the principal values of the integrals, denoted by $\oint$, are taken to obtain the boundary integral equations:

$$f_A(\underline{x}_i) = 2 \oint_{S_I} (f_A(\underline{x})\underline{n}(\underline{x}) \cdot \nabla G(\underline{x}, \underline{x}_i) - G(\underline{x}, \underline{x}_i)\underline{n}(\underline{x}) \cdot \nabla f_A(\underline{x}))\, dS(\underline{x}) \tag{21}$$

$$f_B(\underline{x}_i) = -2 \oint_{S_I} (f_B(\underline{x})\underline{n}(\underline{x}) \cdot \nabla G(\underline{x}, \underline{x}_i) - G(\underline{x}, \underline{x}_i)\underline{n}(\underline{x}) \cdot \nabla f_B(\underline{x}))\, dS(\underline{x}) \tag{22}$$

2.4. The discrete problem

The interface is divided into a number of intervals denoted by subscript j, with $j = 1$ to J. The simplest representation of the solution is chosen, where the boundary is represented by straight line elements and the solution is taken to be piecewise constant. The functions f and the normal derivatives $\underline{n} \cdot \nabla f$ are then represented by the discrete values at the nodes (centres) of each element.

Three different approaches have been used to discretise the interface. For highly curved or circular interfaces, corresponding to a small Bond number and a high contact angle, the nodes are distributed along the interface at regular angular intervals, with equal increments of φ. Where the interface is flat or nearly so, the interface is divided into J elements, with the nodes located at regular intervals along the horizontal axis (x) of the pipe diameter (see Fig. 1). For large Bond numbers, the interface is flat in the centre and highly curved near the ends. In this case, a combination of the nodes obtained from both discretisation methods is used.

Eqs. (21) and (22) are approximated by summations of the exact integrals of $G(\underline{x}, \underline{x}_i)$ and $\underline{n} \cdot \nabla G(\underline{x}, \underline{x}_i)$ over each element of the interface as follows,

$$f_{\mathrm{A}}(\underline{x}_i) \approx 2\sum_{j=1}^{J} f_{\mathrm{A}}(\underline{x}_j) \int_{-S_j/2}^{S_j/2} \underline{n}_j \cdot \nabla G(\underline{x}, \underline{x}_i)\, \mathrm{d}\xi - 2\sum_{j=1}^{J} \underline{n} \cdot \nabla f_{\mathrm{A}}(\underline{x}_j) \int_{-S_j/2}^{S_j/2} G(\underline{x}, \underline{x}_i)\, \mathrm{d}\xi \tag{23}$$

and

$$f_{\mathrm{B}}(\underline{x}_i) \approx -2\sum_{j=1}^{J} f_{\mathrm{B}}(\underline{x}_j) \int_{-S_j/2}^{S_j/2} \underline{n}_j \cdot \nabla G(\underline{x}, \underline{x}_i)\, \mathrm{d}\xi + 2\sum_{j=1}^{J} \underline{n} \cdot \nabla f_{\mathrm{B}}(\underline{x}_j) \int_{-S_j/2}^{S_j/2} G(\underline{x}, \underline{x}_i)\, \mathrm{d}\xi \tag{24}$$

Focusing on a single boundary element, the integrals can be simplified with reference to the sketch shown in Fig. 3. For this purpose, the boundary element, S_j, is re-orientated in a horizontal position, parallel to the ξ-axis. S_j is the length of element j which is bounded by points $\underline{C}_j$ and $\underline{C}_{j+1}$ on the interface. $\underline{t}_j$ and $\underline{n}_j$ are the unit tangent and unit normal to the element. The coordinates of the node $\underline{x}_j$ relative to the point $\underline{x}_i$ are then

$$a = -(\underline{x}_j - \underline{x}_i) \cdot \underline{n}_j$$

$$b = (\underline{x}_j - \underline{x}_i) \cdot \underline{t}_j$$

with similar definitions for $\hat{a}$ and $\hat{b}$ relative to the image point $\underline{\hat{x}}_i$ required for the Green's function. Note that a and b are different for each combination of i and j.

Eqs. (23) and (24) are combined with conditions (14) and (15) for continuity of velocity and shear stress at the interface to obtain a system of equations for the unknown vector $\underline{f}_{\mathrm{A}}$, whose elements are the nodal values $f_{\mathrm{A}i} = f_{\mathrm{A}}(\underline{x}_i)$:

$$\underline{\underline{V}} \cdot \underline{f}_{\mathrm{A}} = \underline{w} \tag{25}$$

where $\underline{\underline{V}}$ is a $(J \times J)$ matrix with elements

$$V_{ij} = \delta_{ij} + \frac{2(1-m)}{(m+1)} H_{ji} \tag{26}$$

Here δ_{ij} is the Kronecker delta and H_{ji} is given by

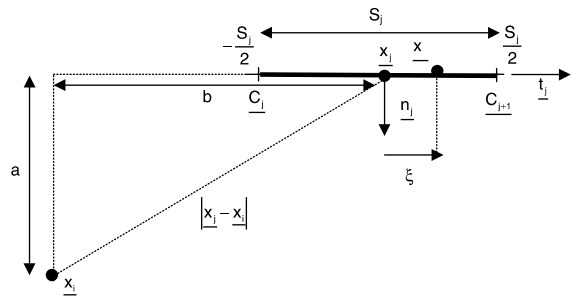

Fig. 3. Schematic diagram of a boundary element used in the evaluation of the integrals.

$$H_{ji} = \int_{-S_j/2}^{S_j/2} \underline{n}_j(\underline{x}) \cdot \nabla G(\underline{x}, \underline{x}_i)\, \mathrm{d}\xi = \frac{1}{2\pi}\left[\tan^{-1}\left(\frac{\hat{b}+\frac{S_j}{2}}{\hat{a}}\right) - \tan^{-1}\left(\frac{b+\frac{S_j}{2}}{a}\right)\right] - \frac{1}{2\pi}\left[\tan^{-1}\left(\frac{\hat{b}-\frac{S_j}{2}}{\hat{a}}\right) - \tan^{-1}\left(\frac{b-\frac{S_j}{2}}{a}\right)\right] \tag{27}$$

The $(J \times 1)$ vector, $\underline{w}$, has elements

$$w_i = \frac{m-\chi}{4m(m+1)}\left(1 - |\underline{x}_i|^2\right) + \frac{1-\chi}{(m+1)}\sum_{j=1}^{J} \underline{n}_j \cdot \underline{x}_j G_{ji} + \frac{m-\chi}{2m(m+1)}\sum_{j=1}^{J}\left(1 - |\underline{x}_j|^2\right) H_{ji} \tag{28}$$

where

$$\begin{aligned} G_{ji} &= \int_{-S_j/2}^{S_j/2} G(\underline{x}, \underline{x}_i)\, \mathrm{d}\xi \\ &= \frac{1}{2\pi}\left(S_j \ln\frac{1}{|\underline{x}_i|}\right) + \frac{1}{2\pi}\left(a\tan^{-1}\left(\frac{b+\frac{S_j}{2}}{a}\right) - a\tan^{-1}\left(\frac{b-\frac{S_j}{2}}{a}\right)\right. \\ &\quad \left. - \hat{a}\tan^{-1}\left(\frac{\hat{b}+\frac{S_j}{2}}{\hat{a}}\right) + \hat{a}\tan^{-1}\left(\frac{\hat{b}-\frac{S_j}{2}}{\hat{a}}\right)\right) \\ &\quad + \frac{1}{2\pi}\left(\left(b+\frac{S_j}{2}\right)\ln\left(\sqrt{a^2 + \left(b+\frac{S_j}{2}\right)^2}\right) - \left(b-\frac{S_j}{2}\right)\ln\left(\sqrt{a^2 + \left(b-\frac{S_j}{2}\right)^2}\right)\right) \\ &\quad - \frac{1}{2\pi}\left(\left(\hat{b}+\frac{S_j}{2}\right)\ln\left(\sqrt{\hat{a}^2 + \left(\hat{b}+\frac{S_j}{2}\right)^2}\right) - \left(\hat{b}-\frac{S_j}{2}\right)\ln\left(\sqrt{\hat{a}^2 + \left(\hat{b}-\frac{S_j}{2}\right)^2}\right)\right) \end{aligned} \tag{29}$$

Once $\underline{f}_A$ is found from Eq. (25), $\underline{f}_B$ can be determined from Eq. (14) and the axial velocities at the interface, u_{zA} and u_{zB} can be calculated.

The values of $\underline{n} \cdot \nabla f_A$ and $\underline{n} \cdot \nabla f_B$ on the interface are required for the prediction of other flow properties of the system. With values of f_A and f_B along the interface known, Eq. (23) can be rearranged to give

$$\underline{\underline{P}} \cdot \underline{F}_A = \underline{q} \tag{30}$$

where $\underline{F}_A$ is a vector of the unknowns, $F_{Ai} = \underline{n} \cdot \nabla f_A(\underline{x}_i)$, $\underline{\underline{P}}$ is a $(J \times J)$ matrix with elements

$$P_{ij} = 2G_{ji} \tag{31}$$

and $\underline{q}$ is a $(J \times 1)$ vector with elements

$$q_i = 2\sum_{j=1}^{J} f_A(\underline{x}_j) H_{ji} - f_A(\underline{x}_i) \tag{32}$$

The nodal values of $(\underline{n} \cdot \nabla f_A)$ are then obtained from Eq. (30) and the values of $(\underline{n} \cdot \nabla f_B)$ from Eq. (15).

2.5. Calculation of the flow rates

The expression for the dimensionless flow rate of fluid A given by

$$Q_{\mathrm{A}} = \int\int_{A} u_{z\mathrm{A}}\,\mathrm{d}A \tag{33}$$

can be converted into a line integral by applying Green's Theorem, Eq. (18), to obtain

$$Q_{\mathrm{A}} = \frac{\chi}{16m}S_{\mathrm{A}} + \int_{S_{\mathrm{I}}}\left(\frac{1}{2}u_{z\mathrm{A}}\underline{n}_{\mathrm{A}}\cdot\underline{x} + \frac{\chi}{16m}(r^2)\underline{n}_{\mathrm{A}}\cdot\underline{x} + \frac{1}{4}(1-r^2)\underline{n}_{\mathrm{A}}\cdot\nabla f_{\mathrm{A}}\right)\mathrm{d}S \tag{34}$$

where S_{A} is the length of the pipe perimeter in contact with fluid A.

The surface integral in Eq. (34) is evaluated using the same technique as in the determination of the interfacial velocities. This gives,

$$\begin{aligned} Q_{\mathrm{A}} \approx & \sum_{j=1}^{J}\left(-\frac{1}{2}u_{z\mathrm{A}}aS_j - \frac{\chi a}{16m}\left[(a^2+b^2)S_j + \frac{1}{12}S_j^3\right]\right) \\ & + \sum_{j=1}^{J}\left(\frac{1}{4}F_{\mathrm{A}j}\left((1-a^2-b^2)S_j - \frac{1}{12}S_j^3\right)\right) + \frac{\chi}{16m}S_{\mathrm{A}} \end{aligned} \tag{35}$$

where the field point $\underline{x}_i$ in the definition of a and b is the centre of the pipe.

Similarly for fluid B, the flow rate, Q_{B}, is approximated by

$$\begin{aligned} Q_{\mathrm{B}} \approx & \sum_{j=1}^{J}\left(\frac{1}{2}u_{z\mathrm{B}}aS_j + \frac{a}{16}\left[(a^2+b^2)S_j + \frac{1}{12}S_j^3\right]\right) \\ & + \sum_{j=1}^{J}\left(\frac{1}{4}F_{\mathrm{B}j}\left((a^2+b^2-1)S_j + \frac{1}{12}S_j^3\right)\right) + \frac{1}{16}S_{\mathrm{B}} \end{aligned} \tag{36}$$

2.6. Calculation of the shear stress

The dimensionless interfacial shear stress is given by

$$\tau_{\mathrm{I}} = m(\underline{n}\cdot\nabla\underline{u}_{z\mathrm{A}}) = \underline{n}\cdot\nabla\underline{u}_{z\mathrm{B}}$$

which is

$$\tau_{\mathrm{I}} = m(\underline{n}\cdot\nabla f_{\mathrm{A}}) - \frac{\chi}{2}\underline{n}\cdot\underline{x} \tag{37}$$

The dimensionless wall shear stress at the boundary of fluid A is

$$\tau_{\mathrm{wA}} = m\left(\frac{\partial f_{\mathrm{A}}}{\partial r}\right)_{r=1} - \frac{\chi}{2} \tag{38}$$

Similarly, the dimensionless wall shear stress at the boundary of fluid B is given by

$$\tau_{wB} = \left(\frac{\partial f_B}{\partial r}\right)_{r=1} - \frac{1}{2} \tag{39}$$

A number of elegant methods are available for finding the shear stress at the wall. However, here, a simple and direct method of finite difference approximation is adopted. Since f is zero at the wall, the value of $\partial f/\partial r$, which is needed for the calculation of the shear stress at the wall can be approximated using the value of f at a point very close to the wall. With $f = 0$ and $r = 1$ at the wall, the following approximation is made

$$\left.\frac{\partial f}{\partial r}\right|_{r=1} \approx -\frac{1}{\delta} f\Big|_{r=1-\delta} \tag{40}$$

This method is very accurate, since the Green's function, Eq. (17), satisfies the wall condition exactly. The results presented below are evaluated with $\delta = 10^{-7}$. However, the wall shear stress at the point where the fluid–fluid interface meets the pipe wall (contact point) cannot be determined by this method. A local analysis of the shear stresses around the contact point is presented in Appendix A.

3. Convergence and comparison with previous results

Before the analysis of the flow predictions obtained via the BEM, it is necessary to confirm the accuracy of this solution scheme. A convergence test has been performed to determine the rate of convergence of the solution with respect to the number of boundary elements or node points on the interface.

Fig. 4 shows the convergence of the dimensionless axial velocity at two points within the fluid with the number of node points on the interface, highlighting the difference between the velocity,

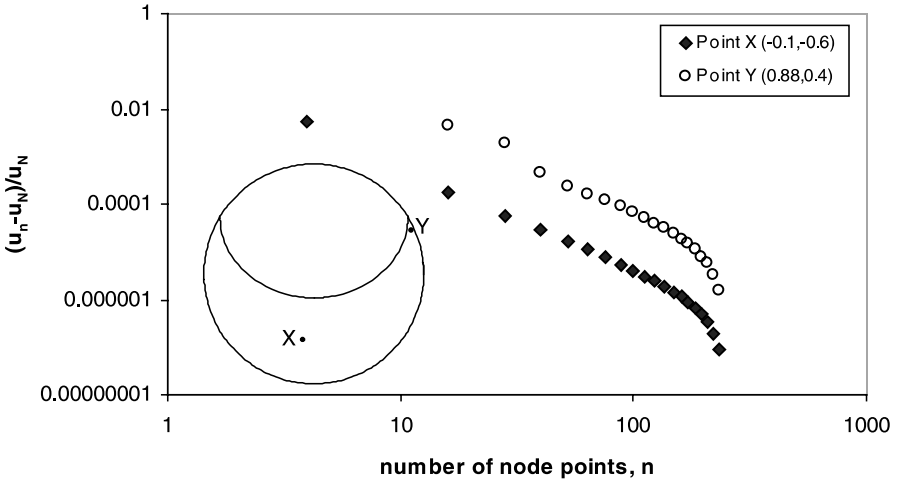

Fig. 4. The convergence of the axial velocity calculated at Points X and Y with increasing number of node points ($\varepsilon = 0.5$, $\theta = \pi/6$, $Bo = 1$, $m = 1.6$, $\chi = 1$).

u_n, evaluated using n node points and the velocity, u_N, using N node points, where N is the largest number of nodes used, plotted on a logarithmic scale. In this flow system ($\varepsilon = 0.5$, $\theta = \pi/6$, $Bo = 1$, $\chi = 1$), the coordinates of the contact points are (± 0.853, 0.522), with the pipe's centre at (0, 0) and a radius of unity. Point X (-0.1, -0.6) is near the symmetry plane in fluid B while Point Y (0.88, 0.4) is near one of the contact points. In this case, the equal angle discretisation is used and N is 244. When a larger number of node points is used, the accuracy of the solution improves, at the expense of increased computational time. A much slower convergence is obtained for Point Y than for Point X, but a rather good approximation (better than 0.1%) to the solution can be obtained by discretising the interface into about 40 boundary elements. It can be concluded that the convergence of the solution is second order, with an error of order $1/n^2$.

The validity of the boundary element calculation has been checked by comparing the solution obtained with the analytical and numerical solutions available in the literature. For all of these comparisons, the interface is flat, and is discretised into 40 elements. This interface shape corresponds to the pseudo-gravity dominated situation described by Gorelik and Brauner (1999) where the surface tension has no effect and the solution is independent of the Bond number. The analytical solution for which comparisons were carried out is for a stratified flow system with a flat interface at a holdup of 50% (Kurban, 1997) while the numerical solution used is the one developed by Hall (1992), applying the bipolar coordinate system. In the latter case, results are compared for planar interfaces at 25% and 75% holdup. The velocities, flow rates, and interfacial and wall shear stresses determined by both methods are compared for a horizontal pipe ($\chi = 1$).

Comparisons with the analytical solution with viscosity ratio $m = 45$ (Kurban, 1997) are shown in Fig. 5 which shows the dimensionless velocity profile on the vertical diameter of the pipe, interfacial shear stress along the horizontal diameter of the pipe, and the wall shear stress around the periphery of the pipe. The flow properties calculated by the BEM agree well with the analytical solution (Kurban, 1997). However, the BEM does not predict the wall shear stress at the contact line. This is dealt with in Appendix A. The dimensionless flow rates for phases A and B calculated by the two different methods are almost identical, as shown in Table 1.

The flow properties obtained using the boundary integral method at 25% and 75% holdup are generally consistent with those calculated from the bipolar numerical solution. The dimensionless volumetric flow rates of fluid A and fluid B for 25% and 75% holdup are compared with the numerical solution by Hall (1992) in Tables 2 and 3 respectively. When the holdup is 75%, the results obtained from the two methods are similar, with a maximum difference of about 5%. For 25% holdup, there is more high viscosity fluid (A) in the pipe and the prediction of its flow rate by the boundary integral method is close to that of the bipolar code. However, when the viscosity ratio is large, the discrepancy in the flow rate of the low viscosity fluid (B) is quite significant, exceeding 20%. This is probably due to the error in the bipolar results. Kurban (1997) compared the bipolar solution to the analytical one for a pseudo-two-phase flow (with the two phases taking the same physical properties, and $m = 1$); the maximum error was around 2% at 75% holdup. This error will increase significantly with viscosity ratio due to the implementation of the equal stress condition on the interface.

Fig. 6 shows the dimensionless velocity profile on the symmetry plane predicted by the BEM for a flat interface with different viscosity ratios. The results are virtually identical to those obtained by Brauner et al. (1996) using the Fourier Integral method. The volumetric flow rates predicted by

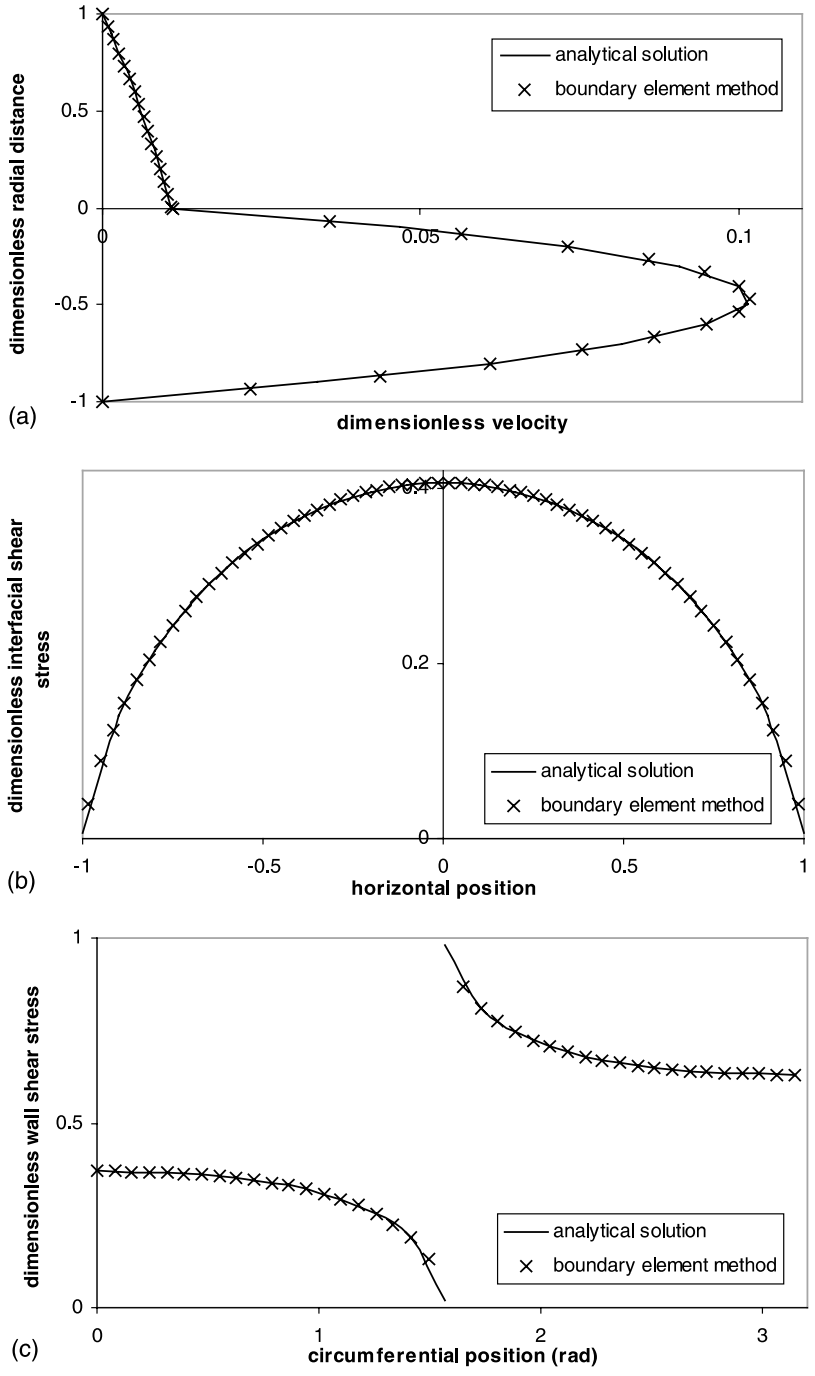

Fig. 5. Comparison of boundary element and exact solutions for a half-filled pipe with a planar interface ($\varepsilon = 0.5$, $m = 45$, $\chi = 1$, $\theta = \pi/2$): (a) velocity profile at the symmetry plane, (b) interfacial shear stress profile and (c) wall shear stress profile.

Table 1
Dimensionless flow rates for a half-filled pipe with a viscosity ratio of 45 ($\varepsilon = 0.5$, $m = 45$, $\chi = 1$, $\theta = \pi/2$)

Fluid	Dimensionless flow rate	
	BEM	Analytical
A	0.00695566	0.00695572
B	0.0796945	0.0796918

Table 2
Dimensionless flow rates for a flat interface at 25% holdup ($\varepsilon = 0.25$, $\chi = 1$)

Viscosity ratio	Dimensionless flow rate of A		Dimensionless flow rate of B	
	BEM	Bipolar code	BEM	Bipolar code
1.6	0.235982	0.238149	0.041802	0.041760
16	0.031651	0.030973	0.012906	0.014576
45	0.011670	0.011354	0.008765	0.010813

Table 3
Dimensionless flow rates for a flat interface at 75% holdup ($\varepsilon = 0.75$, $\chi = 1$)

Viscosity ratio	Dimensionless flow rate of A		Dimensionless flow rate of B	
	BEM	Bipolar code	BEM	Bipolar code
1.6	0.035458	0.035174	0.312456	0.321760
16	0.004567	0.004518	0.242438	0.254013
45	0.001659	0.001641	0.235666	0.247357

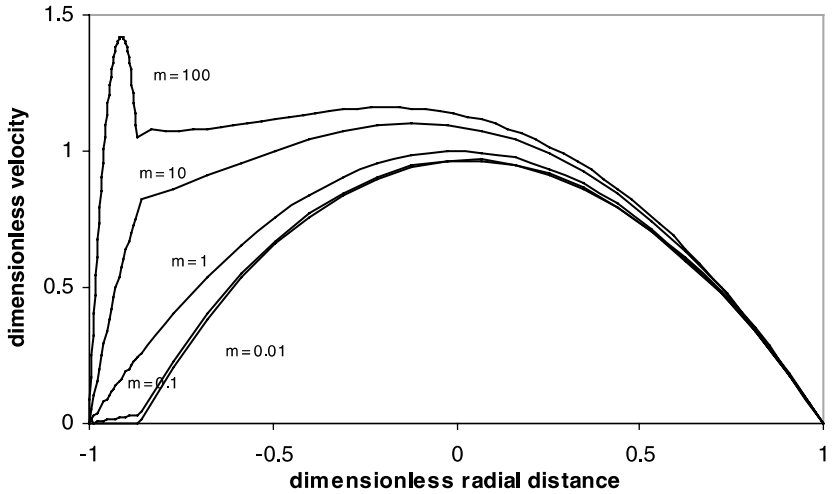

Fig. 6. Dimensionless velocity profile on the symmetry plane for a flat interface and viscosity ratios, $m = 0.01$, 0.1, 1, 10, 100 ($\varepsilon = 0.2$, $\chi = 1$).

the BEM for a flow system with a circular interface have also been found to be indistinguishable from those predicted by Moalem Maron et al. (1995).

4. Results and discussion

When a change is made in the physical properties of the flow system, both the local and the integral flow properties of the system will be altered accordingly. Here, the effects of key parameters on the flow properties are investigated; these are the Bond number, Bo, holdup, ε, contact angle, θ, viscosity ratio, m, and the ratio of the driving forces, χ, for the two fluids. Since there are five independent parameters, it is not possible to present a complete catalogue of solutions. Instead, the effects of changes in parameters relative to a base configuration will be discussed. In all the comparisons and analysis below, the base configuration of the flow system was chosen with a Bond number, $Bo = 10$; contact angle, $\theta = \pi/3$; holdup, $\varepsilon = 0.3$; viscosity ratio, $m = 45$ and driving ratio, $\chi = 1$. The exact interface shape, taking into account the surface tension (Ng et al., 2001), is illustrated in Fig. 2. Here, a rather flat interface was chosen as a reference so that the effects of curvature can be clearly distinguished. In the BEM, the interface is discretised into 40 elements. Only a relatively small number of selected figures are presented. Other results are simply described in the text. Full details are available in Ng et al. (1999a).

The inclination of the pipe affects the properties (and even the direction) of the flow and this can be investigated by manipulating the scaled driving ratio of the flow system, χ, defined in Eq. (5). Pipe inclination is common in subsea pipelines where the seabed is undulating and not flat. In cases where the pipe is in the horizontal position, where gravity is negligible, or where the densities of the top and bottom fluids are equal, χ is unity, and the two-fluids flow co-currently. When χ has a positive value, the two fluids are always in co-current flow. The ways in which the scaled driving ratio χ can change with pipe inclination, α, are shown schematically in Fig. 7. When the pipe is downwardly inclined, χ becomes less than unity, but greater than zero. Hence the flow is always co-current. When the pipe is inclined slightly upwards, α is positive, and hence χ is greater than 1, indicating an upward inclined co-current flow. However, as shown in Fig. 7(a), for small values of the pressure gradient, there is a critical value of α, α_1, when this flow situation changes. The denominator in Eq. (5) reaches zero before the numerator, as the density of fluid B is greater than that of fluid A. As α approaches α_1, χ goes to infinity. Beyond this critical value, χ becomes negative, indicating that the pressure gradient is not strong enough to overcome the weight of the denser fluid which can flow backwards, resulting in counter-current flow. With further increase in the inclination of the pipe, there is a value of α, α_2, when $(-G - \rho_A g \sin\alpha)$ becomes zero. Beyond this point, χ is again positive and the fluids will flow co-currently backwards, against the pressure gradient.

In situations where $\rho_A g < |G| < \rho_B g$, as could occur in laminar gas–liquid flow, the numerator in Eq. (5) is always positive and hence, even for near vertical pipes, counter-current flow is still present, with the denser liquid flowing backwards. This situation may not be stable physically since wave growth and 'flooding' may be initiated. However, in the absence of such flooding effects, the variation of χ with α changes and is indicated in Fig. 7(b). When the pressure gradient is larger than the gravitational terms, χ is always positive so changes in the inclination of the pipe will not affect the direction of the flow, i.e. fluids A and B will always be in co-current flow. This situation is shown in Fig. 7(c).

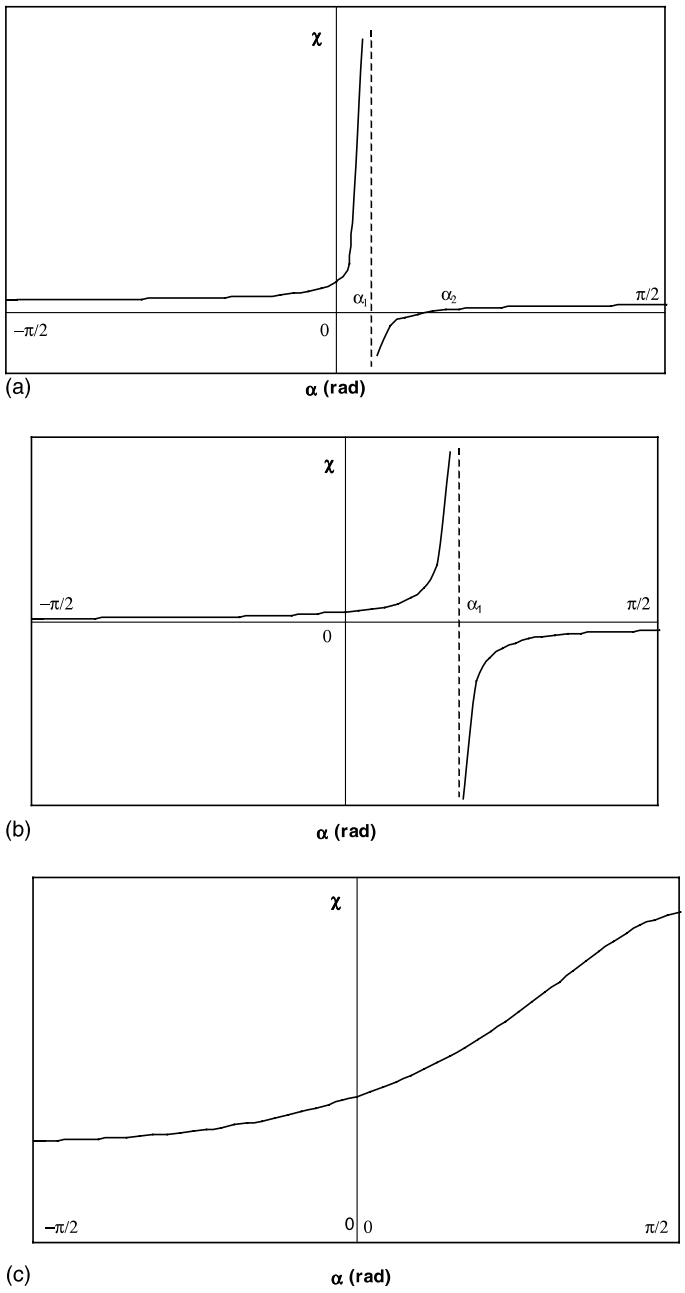

Fig. 7. Schematic graphs of the relationship between χ and α: (a) $|G| < \rho_A g < \rho_B g$, (b) $\rho_A g < |G| < \rho_B g$ and (c) $\rho_A g < \rho_B g < |G|$.

As demonstrated above, all the solutions of the flow problem vary linearly with χ when the other parameters (ε, θ, *Bo* and *m*) are held fixed. This will be evident in the comparisons that follow.

4.1. Interface shape

The parameters which affect the shape of the interface are the Bond number, the holdup and the contact angle of the two fluids and the pipe wall, as outlined in Ng et al. (2001) where a complete catalogue of solutions for the interface shape was presented. As shown in Fig. 2(a), when the holdup of the denser fluid B increases, the interface shape progresses from a convex one to a flat one to a concave one as the pipe is filled. In each case, the thicker line represents the reference configuration. When the holdup increases, the interface becomes highly curved, but its length is greatest around a holdup of 0.5. Increasing the contact angle changes the shape of the fluid–fluid interface from a concave one to a convex one, as shown in Fig. 2(b). As the contact angle increases, the curvature near the walls for the convex interfaces increases and the denser phase forms an eccentric core with the interface curving inwards near the walls. For small values of the Bond number, the interface is a circular arc. As the Bond number increases, the fluid–fluid interface becomes flatter with highly curved menisci at the walls. The length of the interface tends to increase. For the reference values of θ and ε, the interface remains virtually flat for all values of Bo, with only slight changes in the curvature. Changing the viscosity ratio, m, or the driving ratio, χ, does not alter the shape of the interface.

4.2. Interfacial velocity profile

The interfacial velocity increases with increasing holdup until the pipe is approximately half filled with the denser fluid, B. After that, the magnitude of the velocity at the fluid–fluid interface decreases when the holdup of the system is increased further. The highest interfacial velocity corresponds approximately to the longest interface at around 50% holdup.

The velocity at the interface decreases with increasing contact angle, as shown in Fig. 8. There is a peculiarity in the velocity profile at large contact angles approaching π. Near the walls, the

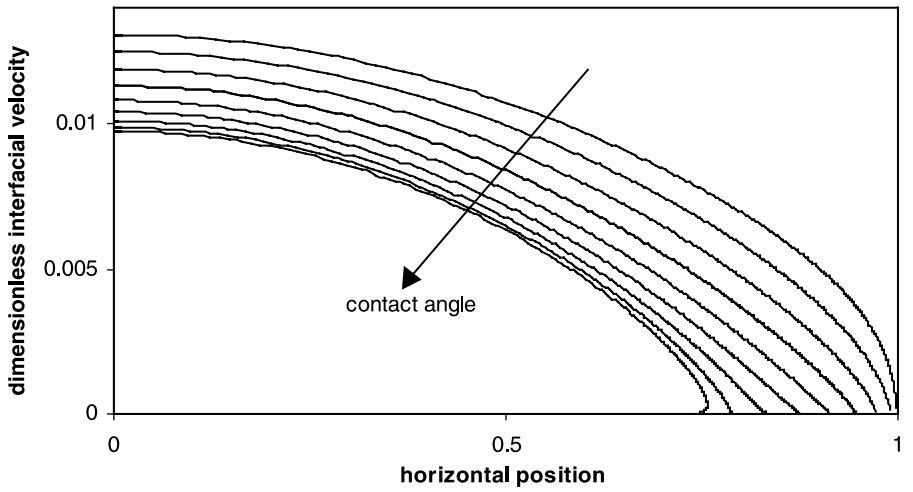

Fig. 8. Variation of the dimensionless interfacial velocity with contact angle, $\theta = 0.1\pi, 0.2\pi, \ldots, 0.9\pi$ ($\varepsilon = 0.3$, $Bo = 10$, $m = 45$, $\chi = 1$).

velocity profiles curve inwards, indicating that there are two values of the interfacial velocity at a particular horizontal position. This is due to the strong curvature of the meniscus in these cases where the interface curves back on itself, as seen in Fig. 2(b).

4.3. Velocity profile in the symmetry plane

The maximum velocity generally occurs in the denser, less viscous fluid B, and increases with the holdup. At a viscosity ratio of 45, the lower fluid moves much more easily than the upper fluid. When the viscosity ratio differs significantly from unity, the flow in the more viscous phase resembles shear driven flow, while the less viscous phase flows as if the interface is a solid wall. When the viscosity ratio is unity, the velocity profile is parabolic. In this case, the two phases act as a single fluid, and the highest velocity is at the centre of the pipe.

Fig. 9 shows the velocity profile across the whole pipe for a case with viscosity ratio of 45, holdup of 0.5, and Bond number of 1. The variation of the velocity in each phase is roughly parabolic in all directions, as would be expected.

Fig. 10 shows the effect of variation of the driving ratio on the dimensionless velocity profile at the symmetry plane. The change in dimensionless velocity is linear with respect to the driving ratio. When the scaled driving ratio increases (Fig. 10(a)), the velocities increase correspondingly, but the change in magnitude of the dimensionless velocity for each step change of χ is greater in the top fluid than in the bottom fluid. Fig. 10(b) shows the velocity profiles for cases when $\chi = 0$, -1, -2, -3, -4 and -5. The dimensionless velocity is scaled with U, defined in Eq. (6), which is negative when χ is less than or equal to zero, so the velocity has been multiplied by -1 to obtain the correct flow direction, which is equivalent to scaling with the magnitude of the velocity scale, $|U|$. In this case, the flows are counter-current, with the denser fluid flowing backwards. At $\chi = 0$, reverse flow occurs, with both fluids flowing backwards in a greatly inclined pipe.

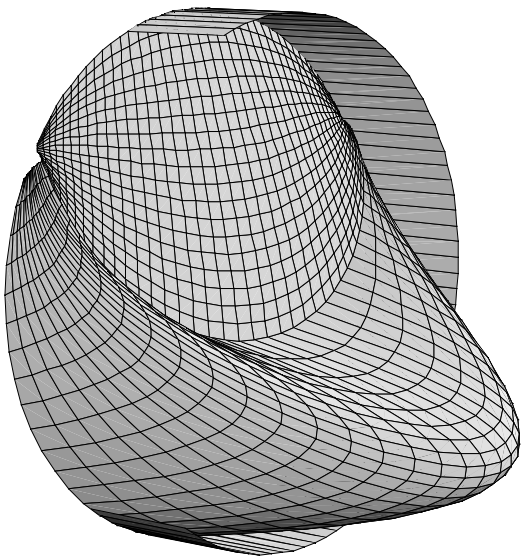

Fig. 9. Velocity profile across the pipe cross-section ($\varepsilon = 0.5$, $\theta = \pi/6$, $Bo = 1$, $\chi = 1$, $m = 45$).

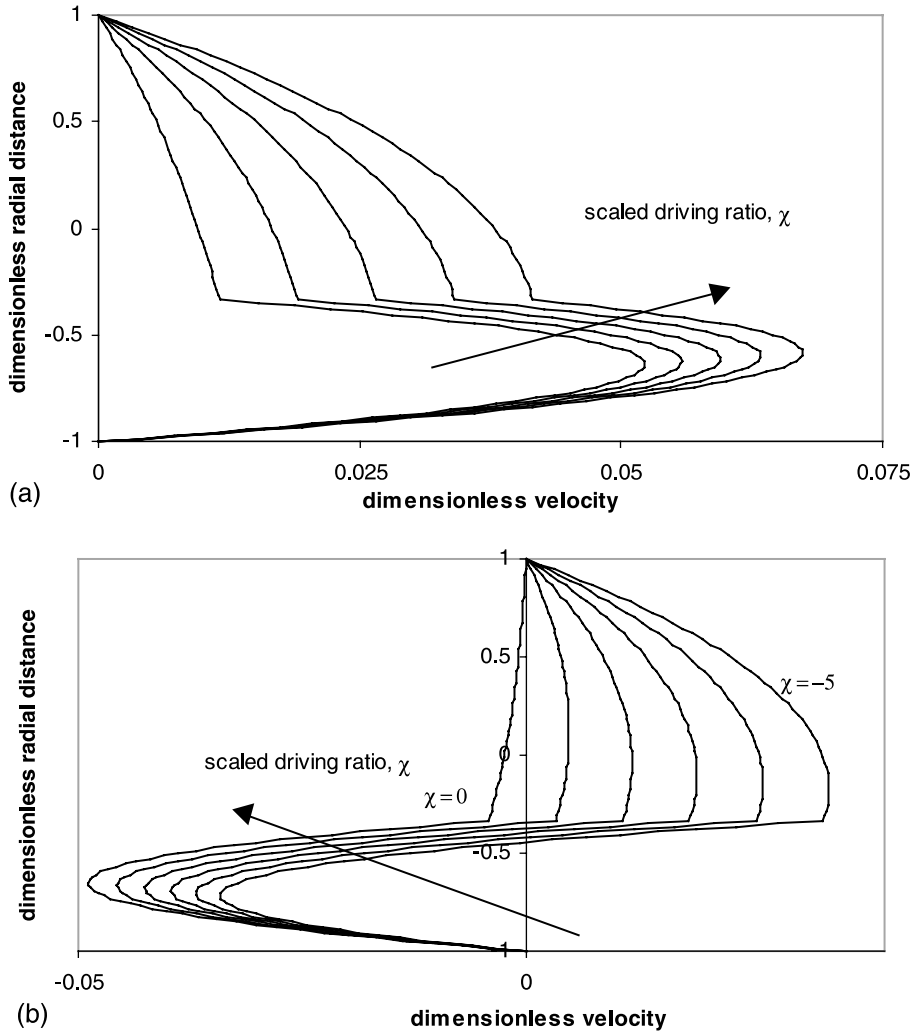

Fig. 10. Variation of the dimensionless velocity profile at the symmetry plane with the scaled driving ratio ($\varepsilon = 0.3$, $\theta = \pi/3$, $Bo = 10$, $m = 45$): (a) $\chi = 1, 2, 3, 4, 5$, (b) $\chi = -5, -4, -3, -2, -1, 0$ (the sign of the velocity is adjusted).

4.4. Interfacial shear stress

When the holdup of the denser fluid increases, the difference between the interfacial shear stress at the walls and the centre of the pipe increases, as shown in Fig. 11(a). Like the interfacial velocity, the shear stress at the interface is symmetrical across the vertical diameter. The maximum velocity occurs near the centre of area of fluid B. Hence when the holdup increases, the velocity difference across the interface increases dramatically, increasing the magnitude of the interfacial shear stress. The interface becomes shorter in length and more curved when the holdup increases beyond 50%.

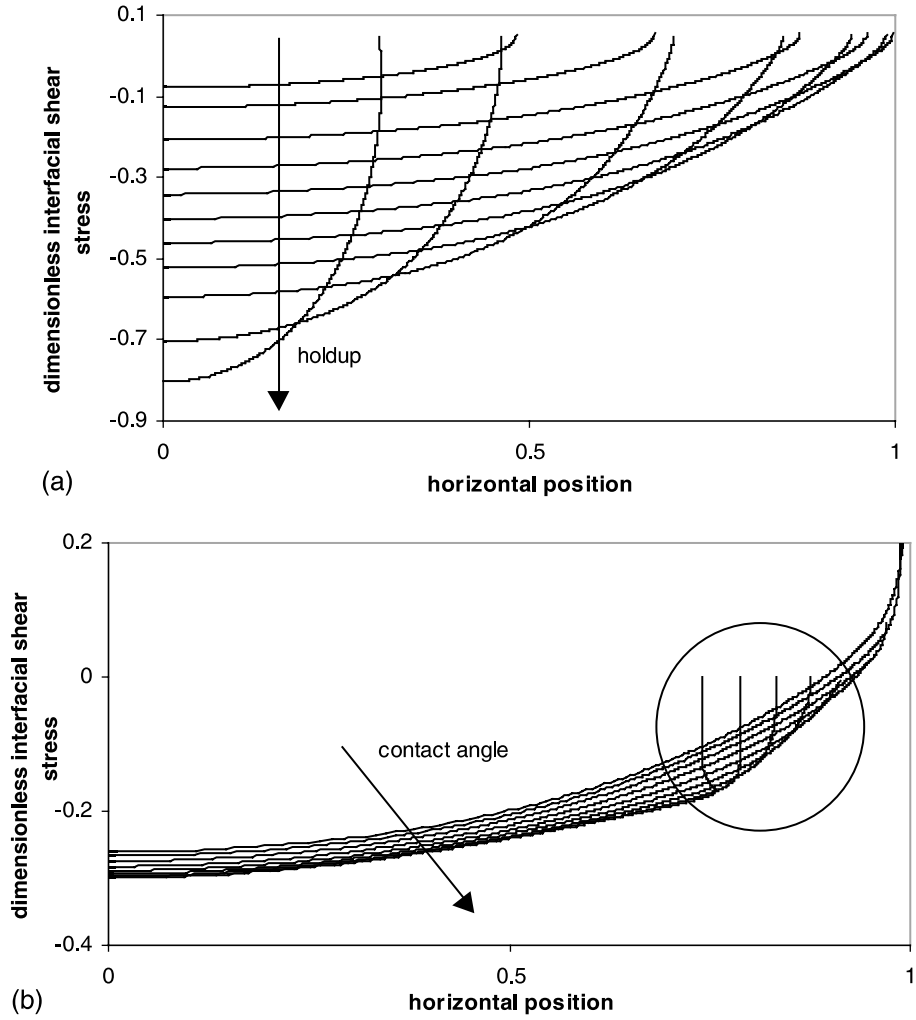

Fig. 11. Variation of the dimensionless interfacial shear stress (a) with holdup, $\varepsilon = 0.05, 0.1, 0.2, \ldots, 0.9, 0.95$ ($\theta = \pi/3$, $Bo = 10$, $m = 45$, $\chi = 1$) and (b) with contact angle, $\theta = 0.1\pi, 0.2\pi, \ldots, 0.9\pi$ ($\varepsilon = 0.3$, $Bo = 10$, $m = 45$, $\chi = 1$).

The interfacial shear stress is not strongly affected by variation of the contact angle, as seen in Fig. 11(b). When the contact angle between the two fluids and the wall approaches π, the interface position becomes multi-valued and there are two values of the interfacial shear stress at a single position near the pipe wall. At such high contact angles, the less viscous phase, fluid B, begins to curl up into an eccentric core. In general, the dimensionless interfacial shear stress decreases when the contact angle increases; this corresponds to the decrease in the velocity at the interface shown in Fig. 8. In addition, the interfacial shear stress increases steeply towards the wall. This is related to the discontinuity in the wall shear stress across the interface. The local analysis of the interfacial shear stresses, outlined in Appendix A, shows that when the contact angle is greater than $\pi/2$, the interfacial shear stress on the wall is zero; this is indicated in the figure. When the contact angle is less than $\pi/2$, the interfacial shear stress tends to infinity at the contact point.

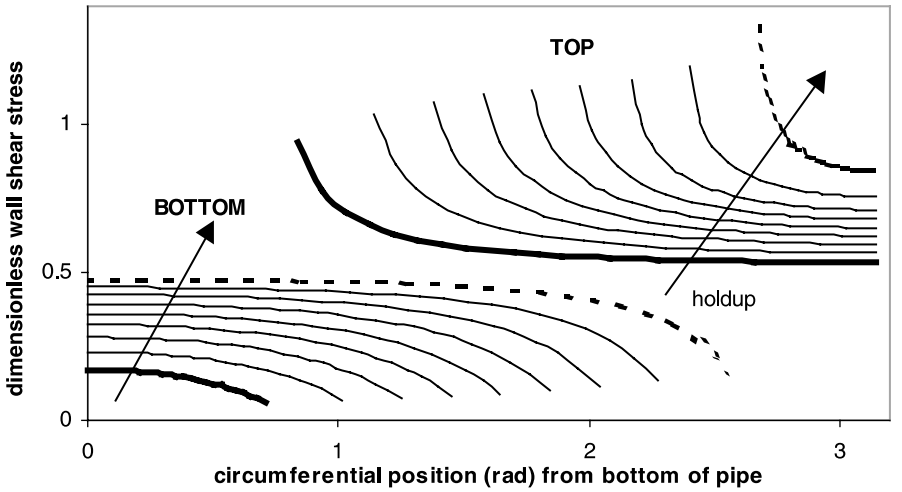

Fig. 12. Variation of the dimensionless wall shear stress profile with holdup, $\varepsilon = 0.1, 0.2, \ldots, 0.9$ ($\theta = \pi/3$, $Bo = 10$, $m = 45$, $\chi = 1$).

The shear stress at the interface decreases with increasing viscosity ratio. When the viscosity ratio is large, the interfacial stress is negative and decreases in magnitude towards the wall. Near the walls, the change in shear stress on the interface is quite rapid, influenced by the effect of the shear stress at the walls. When the viscosity ratio is unity, the interfacial shear stress is approximately constant in value, with a slight increase in value near the walls.

4.5. Wall shear stress

The variation of the dimensionless shear stress around the pipe wall is illustrated in Fig. 12. Here, the shear stress is made dimensionless by dividing by $\mu_B U/R = (-G - \rho_B g \sin\alpha)R$. The section labelled 'TOP' in the graph shows the wall shear stress profile in the more viscous fluid A, while the 'BOTTOM' section represents the wall shear stress in the less viscous lower phase. The two parts are not symmetrical to each other, with the shear stress around both the top and bottom walls being roughly constant except near the contact point, where there is a discontinuity. The wall shear stress in the less viscous lower layer is less than that in the upper fluid. As the denser fluid is less viscous, it flows at a higher velocity, and hence exerts a positive drag on the upper fluid. Since the forces must balance, the stress on the wall is therefore higher for the upper fluid. When the holdup increases, the wall shear stress increases in both fluids, but the average shear stress, integrated around the pipe wall remains constant, with value 0.5, as required from a global force balance.

When the pipe is inclined, the buoyancy of the upper fluid affects the global momentum balance, so the average wall shear stress changes with χ. Fig. 13 shows the effect of χ on the dimensionless wall shear stress. The cases of $\chi \leqslant 0$ are shown with the sign adjusted in Fig. 13(b). In the top fluid, the shear stress on the wall is approximately constant except in the region near the contact line. When the driving ratio is negative, the wall shear stresses in fluids A and B are of opposite sign, indicating that counter-current flow is present.

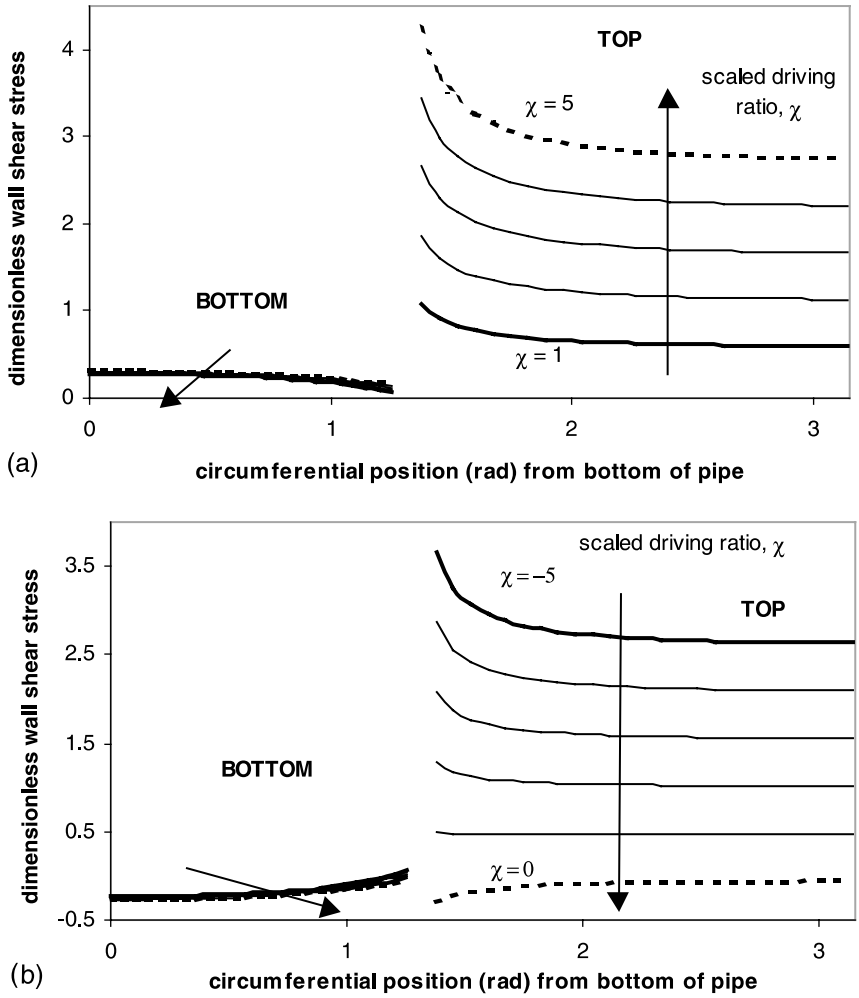

Fig. 13. Variation of the dimensionless wall shear stress profile with the scaled driving ratio ($\varepsilon = 0.3$, $\theta = \pi/3$, $Bo = 10$, $m = 45$): (a) $\chi = 1, 2, 3, 4, 5$ and (b) $\chi = -5, -4, -3, -2, -1, 0$ (the sign is adjusted).

When the viscosity ratio is unity, the wall shear stress around the whole periphery of the pipe has a constant value of 0.5 since the two separate phases act as a single fluid. The wall shear stress of the upper fluid increases in value when the viscosity ratio is increased. The value is approximately constant around most of the wall but increases near the contact point for a viscosity ratio greater than one. There is not much change in the trend of the wall shear stress in the denser fluid B; it decreases in value when the viscosity ratio is increased. For horizontal flows, $\chi = 1$, it consistently decreases in value when the contact point is approached.

4.6. Volumetric flow rate

The volumetric flow is made dimensionless by dividing by UR^2, which is equal to $(-G - \rho_B g \sin\alpha)R^4/\mu_B$. The effects of holdup and Bond number on the dimensionless flow rates of

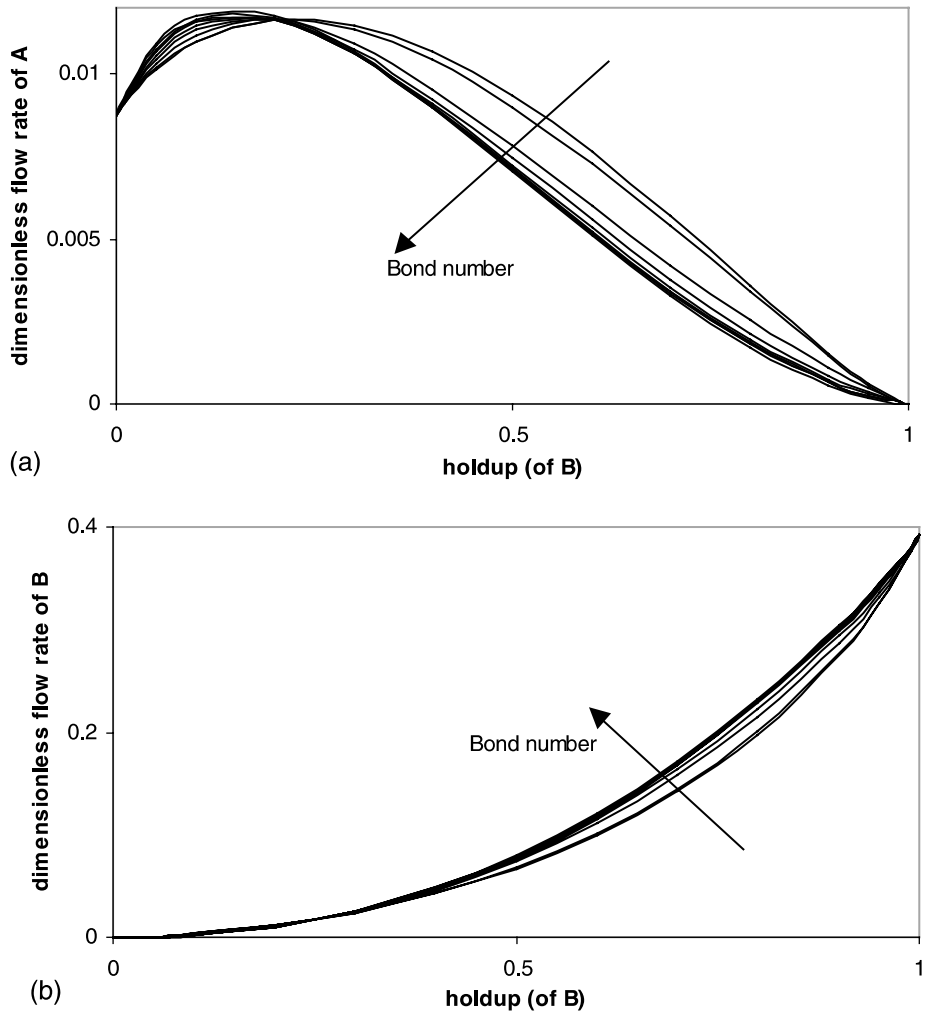

Fig. 14. Variation of the dimensionless flow rate with holdup and Bond number, $Bo = 0.1, 1, 10, 25, 50, 75, 100, 150, 200$ ($\theta = \pi/3$, $m = 45$, $\chi = 1$): (a) fluid A and (b) fluid B.

fluids A and B are illustrated in Fig. 14. The flow rate is roughly proportional to the cross-sectional area of the flow, so generally the larger the cross-sectional area, the higher the flow rate. The two graphs are of different shapes due to the large viscosity ratio. The maximum dimensionless flow rate of fluid B is $\pi/8$, corresponding to a full pipe, while the dimensionless flow rate of fluid A when it fills the pipe is $\pi/360$. There is a maximum flow rate for the more viscous upper fluid A at approximately 20–25% holdup. This is because when the holdup (of B) is small, the cross-sectional area of the more viscous fluid remains large, but the contact periphery with the wall is reduced. The flow in fluid A is similar to a shear driven flow, with the interfacial shear contributing an additional driving force. This feature can also be seen in the results of Davis and Mai (1991) and Ranger and Davis (1979). They performed computational studies on the

volumetric flux of both Newtonian and non-Newtonian fluids (with a flat interface). Their numerical results showed that the flux is higher when the pipe is around 75% filled than when the pipe is completely filled.

The flow rate of the more viscous phase A generally decreases with increasing Bond number as can be observed in Fig. 14(a). Beyond a Bond number of approximately 80, there is no significant change in the volumetric flow rate, as indicated by the thick band of curves. The dimensionless volumetric flow rate of the less viscous phase, fluid B, increases slightly with Bond number as can be seen from Fig. 14(b).

Fig. 15(a) illustrates the decrease in volumetric flow rate of the top fluid with increasing contact angle of the flow system while Fig. 15(b) shows the corresponding small increase in the flow of fluid B. The trends can be explained by the change in the wetted perimeter of the fluids. As the

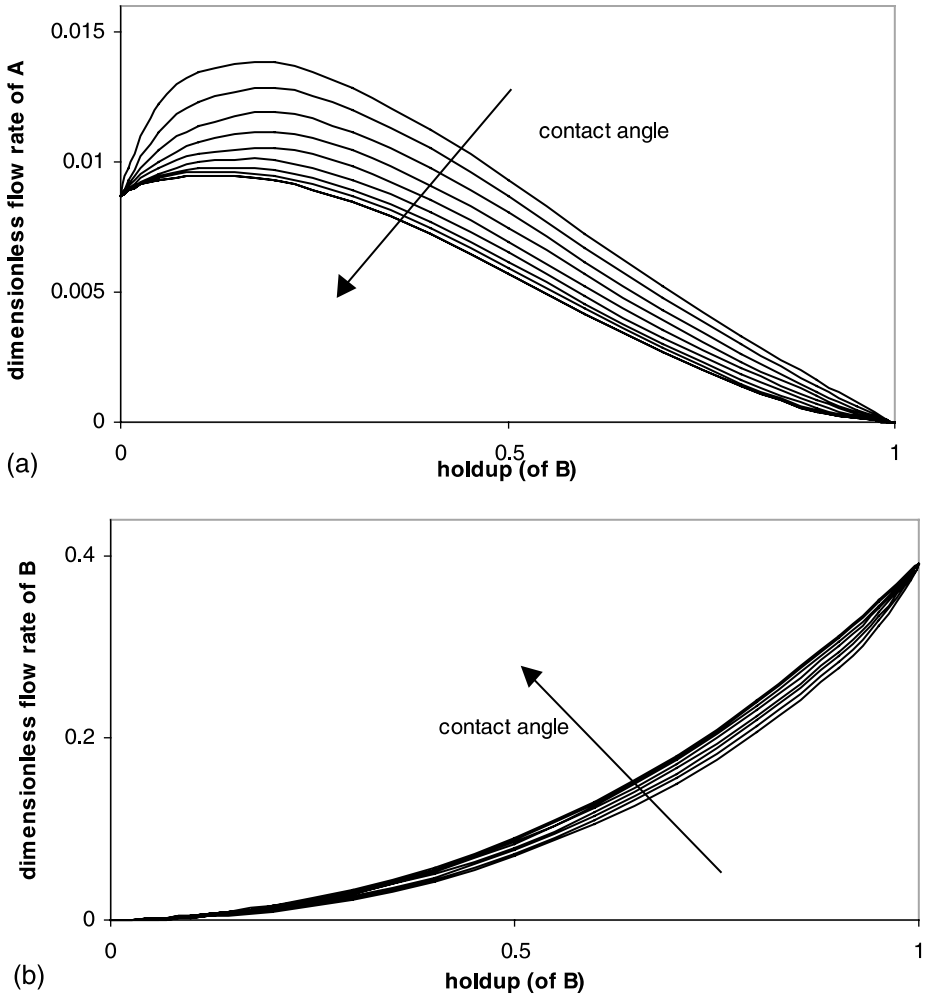

Fig. 15. Variation of the dimensionless flow rate with holdup and contact angle, $\theta = 0.1\pi, 0.2\pi, \ldots, 0.9\pi$ ($Bo = 10$, $m = 45$, $\chi = 1$): (a) fluid A and (b) fluid B.

contact angle increases, fluid B forms an eccentric core, with an increasing flow rate, while the contact perimeter of fluid A increases. The interfacial shear stress is reduced, and hence the flow rate of fluid A decreases. Here, the variation of flow rate of phase A with respect to holdup follows the same trend as observed in Fig. 14(a). The change in flow rate of fluid A with contact angle is again more significant than that of the less viscous fluid B.

Fig. 16 indicates the variation of the dimensionless flow rates of A and B with respect to the scaled driving ratio, χ. Fig. 16(c) and (d) show the variation of the dimensionless flow rates after the sign has been adjusted for χ less than or equal to zero. The change in the dimensionless flow rates is linear with the change in χ. The magnitude of the dimensionless flow rate of A increases with the magnitude of χ. When χ takes the value zero, the pipe is inclined upwards and A is flowing backwards, the shape of the graph is nearly symmetrical, with the maximum flow rate very near 50% holdup.

Because of the chosen scaling, there is very little change in the magnitude of the dimensionless volumetric flow rate of fluid B with variation of the driving ratio, as illustrated in Fig. 16(b) and (d). In general, the dimensionless flow rate of B increases vary slightly with increasing χ. When the driving ratio is negative, counter-current flow occurs, and fluid B is flowing backwards, as indicated by the negative flow rates in Fig. 16(d).

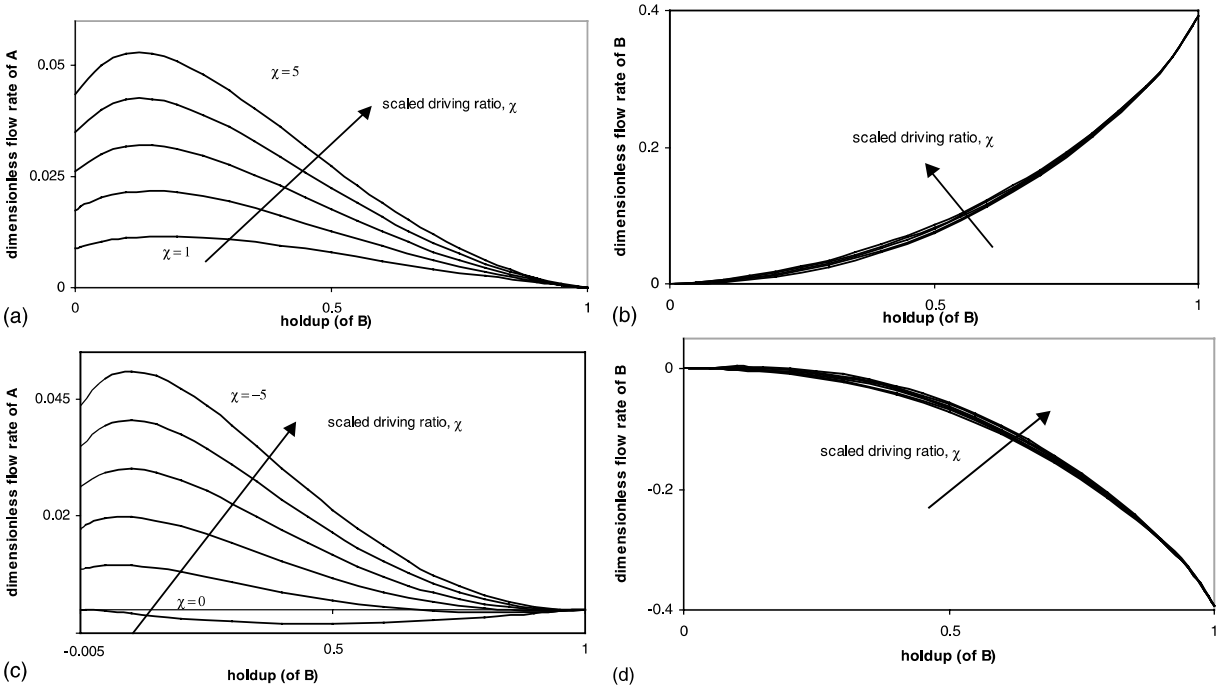

Fig. 16. Variation of the dimensionless flow rate with holdup and scaled driving ratio ($\theta = \pi/3$, $Bo = 10$, $m = 45$): (a) fluid A, $\chi = 1, 2, 3, 4, 5$; (b) fluid B, $\chi = 1, 2, 3, 4, 5$; (c) fluid A, $\chi = -5, -4, -3, -2, -1, 0$ (the sign is adjusted) and (d) fluid B, $\chi = -5, -4, -3, -2, -1, 0$ (the sign is adjusted).

5. Conclusion

The most important integral flow properties, from the industrial and practical perspective, are the volumetric flow rates of the two fluids. For example this information could be used to determine the optimal amount of water to be injected to minimise the energy requirements for oil transportation in pipelines.

In the BEM, only the integrals on the boundary (fluid–fluid interface) need to be evaluated to determine all the integral and local flow properties of the physical flow system. As integrals over the flow domain are not required in the calculations, the computational time is very short. The method is highly efficient for determining the flow properties of two-phase laminar–laminar pipe flow.

The results for all flow properties obtained from the BEM agree well with the analytical solution (Kurban, 1997) for a pipe with a flat interface at 50% holdup. In the comparison against the bipolar finite difference results of Hall (1992) for flat interfaces at 25% and 75% holdup, the two methods agree reasonably well, but with a maximum error of 20% in the flow rates at a viscosity ratio of 45. This is due to the large error present in the bipolar code. In addition, the boundary element solutions compare well with those obtained via the Fourier integral method by Brauner et al. (1996) for circular interfaces.

The local and integral flow properties of the fluid flow system are determined by the shape of the interface which depends on the key physical parameters (the Bond number, Bo, the contact angle, θ, and the holdup, ε) of the physical flow system as well as by the inclination of the pipe and the viscosity ratio. The flow properties have a linear dependence on the driving ratio, χ, which is related to the inclination of the pipe.

The current work has addressed the calculation of the velocity fields, shear stresses and flow rates for fully developed, laminar stratified flows in which the interface remains free of waves and other disturbances. In this calculation, the Reynolds number has no effect, since the flow is perfectly parallel. The stability of these flows is not discussed here. In general, one would expect to find instabilities and transitions to more complex flows, associated with critical values of some of the parameters. Such instabilities could include shear flow instability of the less viscous phase at high Reynolds number, the occurrence of interfacial waves at high Froude number, and capillary instabilities at low values of the Bond number. The present work could be used as a starting point for the analysis of such transitions.

Acknowledgements

This work was supported by the WASP Consortium. We would like to thank Professor Costas Pozrikidis for helpful discussion.

Appendix A. Behaviour of the shear stresses near the contact line

The behaviour of the shear stresses near the contact line is investigated using a local polar coordinate system (s, ϕ) centred at the contact point C, as shown in Fig. 17.

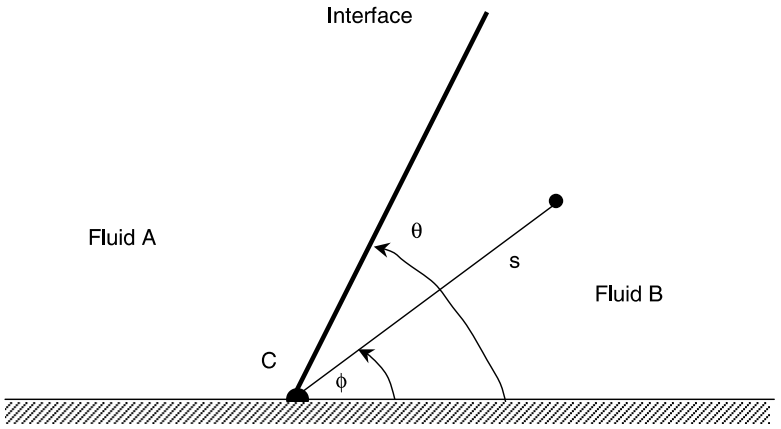

Fig. 17. The local (s, ϕ) coordinate system at the contact line.

The governing equations and boundary conditions are

$$\nabla^2 f_i = 0 \quad \text{in region } i,\ i = \text{A or B} \tag{A.1}$$

with

$$f_i = 0 \quad \text{on } S_i\ (\phi = 0 \text{ or } \phi = \pi) \tag{A.2}$$

On the interface S_I,

$$f_\text{A} - f_\text{B} = \frac{m - \chi}{4m}\left(1 - r^2\right) \tag{A.3}$$

$$m(\underline{n} \cdot \nabla f_\text{A}) - \underline{n} \cdot \nabla f_\text{B} = \frac{\chi - 1}{2}\underline{n} \cdot \underline{x} \tag{A.4}$$

In the local polar coordinate system, the latter conditions are applied at $\phi = \theta$, and approximated as

$$f_\text{A} - f_\text{B} = \frac{m - \chi}{4m} s \sin\theta \tag{A.5}$$

$$m\frac{\partial f_\text{A}}{\partial \phi} - \frac{\partial f_\text{B}}{\partial \phi} = \frac{\chi - 1}{2} s \cos\theta \tag{A.6}$$

A particular solution of this system is

$$f_\text{A}^\text{P} = -\frac{\chi}{2m} s \sin\phi \tag{A.7}$$

$$f_\text{B}^\text{P} = -\frac{1}{2} s \sin\phi \tag{A.8}$$

However this solution is such that the wall and interface stresses given by

$$\tau_{wA} = \frac{m}{s}\left(\frac{\partial f_A}{\partial \phi}\right)_{\phi=\pi} - \frac{\chi}{2} \tag{A.9}$$

$$\tau_{wB} = -\frac{1}{s}\left(\frac{\partial f_B}{\partial \phi}\right)_{\phi=0} - \frac{1}{2} \tag{A.10}$$

$$\tau_I = -\frac{m}{s}\left(\frac{\partial f_A}{\partial \phi}\right)_{\phi=\theta} - \frac{\chi}{2}\cos\theta \tag{A.11}$$

are all identically zero.

Hence the stresses of interest are given by the dominant behaviour of the homogenous solution of Eqs. (A.1)–(A.6). The homogenous solution has terms of the form:

$$f_A^H = -\frac{c}{\lambda}\frac{\sin\lambda\theta}{\sin\lambda(\pi-\theta)} s^\lambda \sin\lambda(\pi-\phi) \tag{A.12}$$

$$f_B^H = -\frac{c}{\lambda} s^\lambda \sin\lambda\phi \tag{A.13}$$

where c is an arbitrary constant, and the value of λ is determined by the transcendental equation

$$m = -\frac{\tan\lambda(\pi-\theta)}{\tan\lambda\theta} \tag{A.14}$$

The homogenous solution gives contributions to the stresses of the form

$$\tau_{wA} = cs^{\lambda-1}\frac{m\sin\lambda\theta}{\sin\lambda(\pi-\theta)} \tag{A.15}$$

$$\tau_{wB} = cs^{\lambda-1} \tag{A.16}$$

$$\tau_I = cs^{\lambda-1}\cos\lambda\theta \tag{A.17}$$

The boundary conditions (A.2) require λ to be positive so that $f \to 0$ as $s \to 0$. Hence, we are interested in the smallest positive solution of Eq. (A.14) for λ. As Eq. (A.14) has symmetry with respect to the replacements, $m \to 1/m$ and $\theta \to \pi - \theta$, it is sufficient to consider cases for $m > 1$. The set of solutions is shown in Fig. 18 for selected values of m. The pattern of the solution is clear and divides into two cases. In case I, $m > 1$ and $0 < \theta < \pi/2$ (or $m < 1$ and $\pi/2 < \theta < \pi$), the value of λ is less than unity. Thus, when the more viscous fluid occupies the obtuse angle, the stress at the contact line is singular; this is similar to the case of the more viscous fluid with a free surface. In case II, $m > 1$ and $\pi/2 < \theta < \pi$ (or $m < 1$ and $0 < \theta < \pi/2$), the value of λ is greater than unity. Thus, when the less viscous fluid occupies the obtuse angle, the stress at the contact line is zero; this is similar to the case of the less viscous fluid flowing in a solid re-entrant corner.

It is noted that, even for $m = 40$, the value of λ does not vary greatly from unity, so the singularity in case I is rather weak, and the approach to zero in case II is rather abrupt.

There are four special cases: $m = 1$, $\theta = 0$, $\theta = \pi/2$, and $\theta = \pi$, for which λ takes the value of unity. When $m = 1$, all of the stresses remain finite, and the wall shear stress is continuous across the interface, $\tau_{wA} = \tau_{wB}$. When $\theta \to 0$ or $\theta \to \pi$, the stresses tend to a finite limit with $\tau_{wA} = \tau_{wB} = |\tau_I|$; the contact point acts as a point on a plane solid wall. When $\theta = \pi/2$, the in-

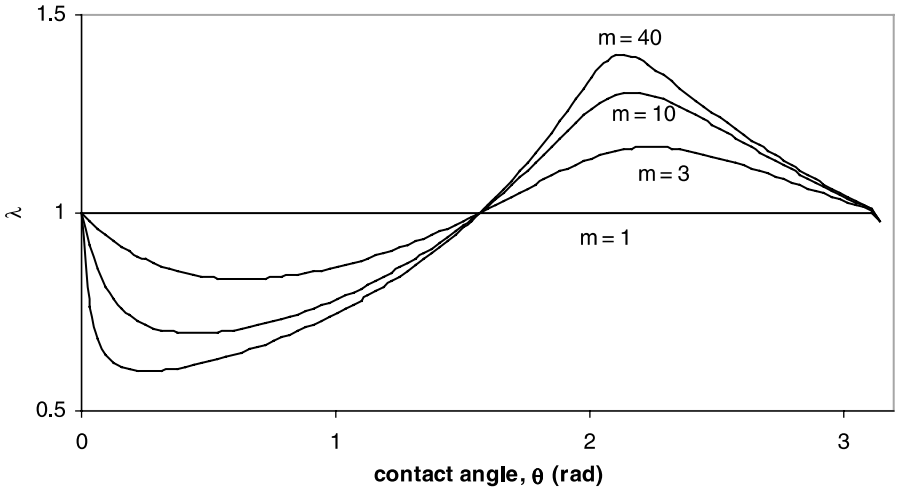

Fig. 18. The variation of λ with θ for $m = 1$, 3, 10 and 40.

terface stress τ_I is zero, and the wall shear stresses are related by $\tau_{wA} = m\ \tau_{wB}$. This result is consistent with that for the case of a flat diametrical interface (e.g. Biberg and Halvorsen, 2000) where the dimensionless wall shear stresses, expressed in terms of our notation are

$$\tau_A = \frac{m}{2}\left(\frac{1+\chi}{1+m}\right) \tag{A.18}$$

$$\tau_B = \frac{1}{2}\left(\frac{1+\chi}{1+m}\right) \tag{A.19}$$

The two principal cases outlined above are of general interest in the present work. In case II, the stresses approach zero at the contact point. Thus, the limiting stress is known, and this value is included in Fig. 11(b). In case I, the stresses are all singular at the contact point, and thus cannot be shown on the figures. However, a representative case ($\varepsilon = 0.3$, $\theta = \pi/3$, $Bo = 10$, $m = 40$ and $\chi = 1$) is shown in Fig. 19. The logarithmic plots show that the stresses adopt a power-law form for small s, whose slope λ agrees with the value 0.76 determined from Eq. (A.14) and whose intercepts agree reasonably well with Eqs. (A.15)–(A.17) when c is set equal to 0.022. Fig. 20 shows the slow approach to zero (on a logarithmic scale) of the stresses in case II. In this example, ($\varepsilon = 0.3$, $\theta = 2\pi/3$, $Bo = 10$, $m = 40$, $\chi = 1$), λ takes the value 1.39 and the constant c is set to 0.37. The stresses predicted by the BEM and the local analysis again agree reasonably well in the region of the contact point. It is noted that the interfacial shear stress is negative in this case, from Eq. (A.17), and so the magnitude of the shear stress is plotted in Fig. 20(c).

A general discussion of the stresses near the contact line has recently been given by Biberg and Halvorsen (2000). The limiting behaviour of the wall and interfacial shear stress at the contact line was obtained by residue calculus. The results are similar to those presented here, but less succinct.

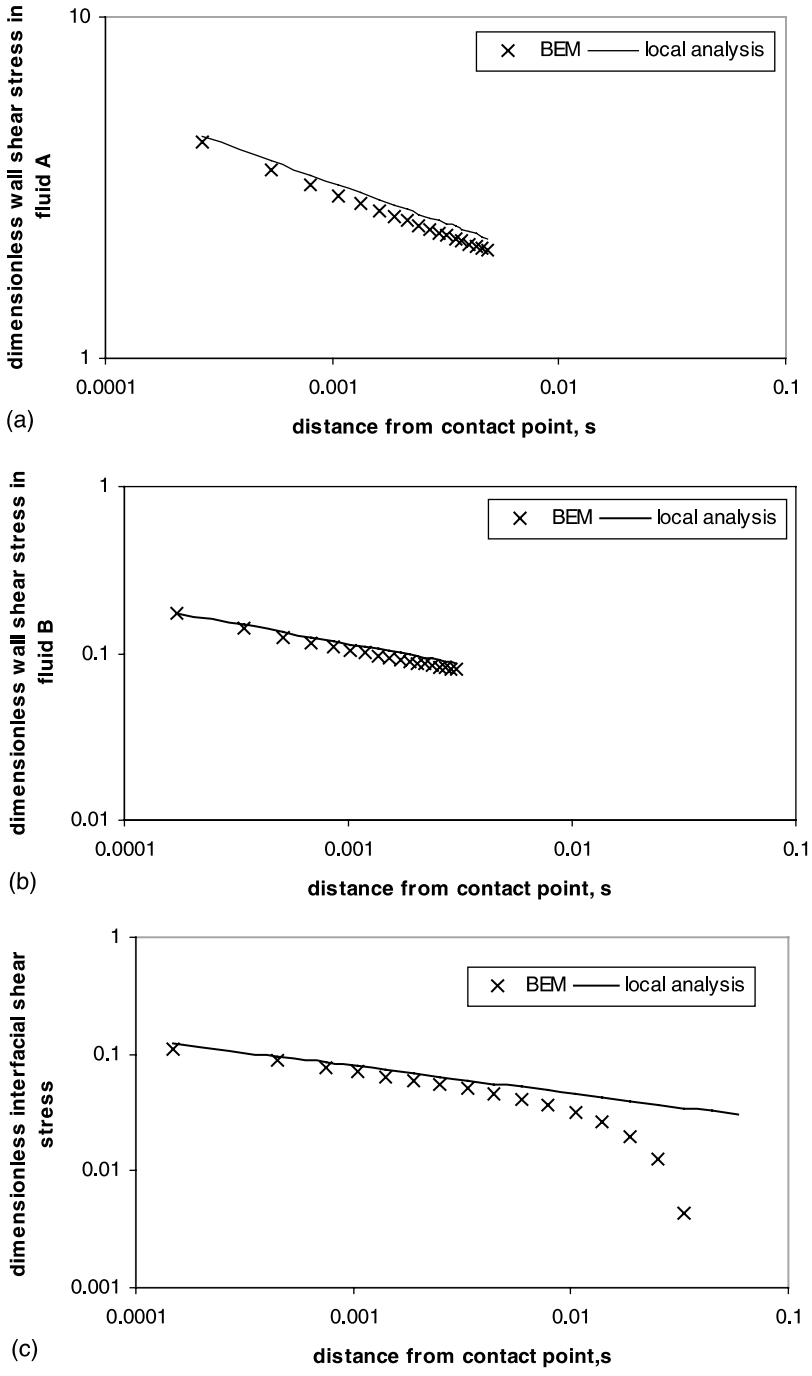

Fig. 19. The variation of the dimensionless shear stress with distance from the contact point, Case I stress increases ($\varepsilon = 0.3$, $\theta = \pi/3$, $Bo = 10$, $m = 40$, $\chi = 1$): (a) wall shear stress in fluid A, (b) wall shear stress in fluid B and (c) interfacial shear stress.

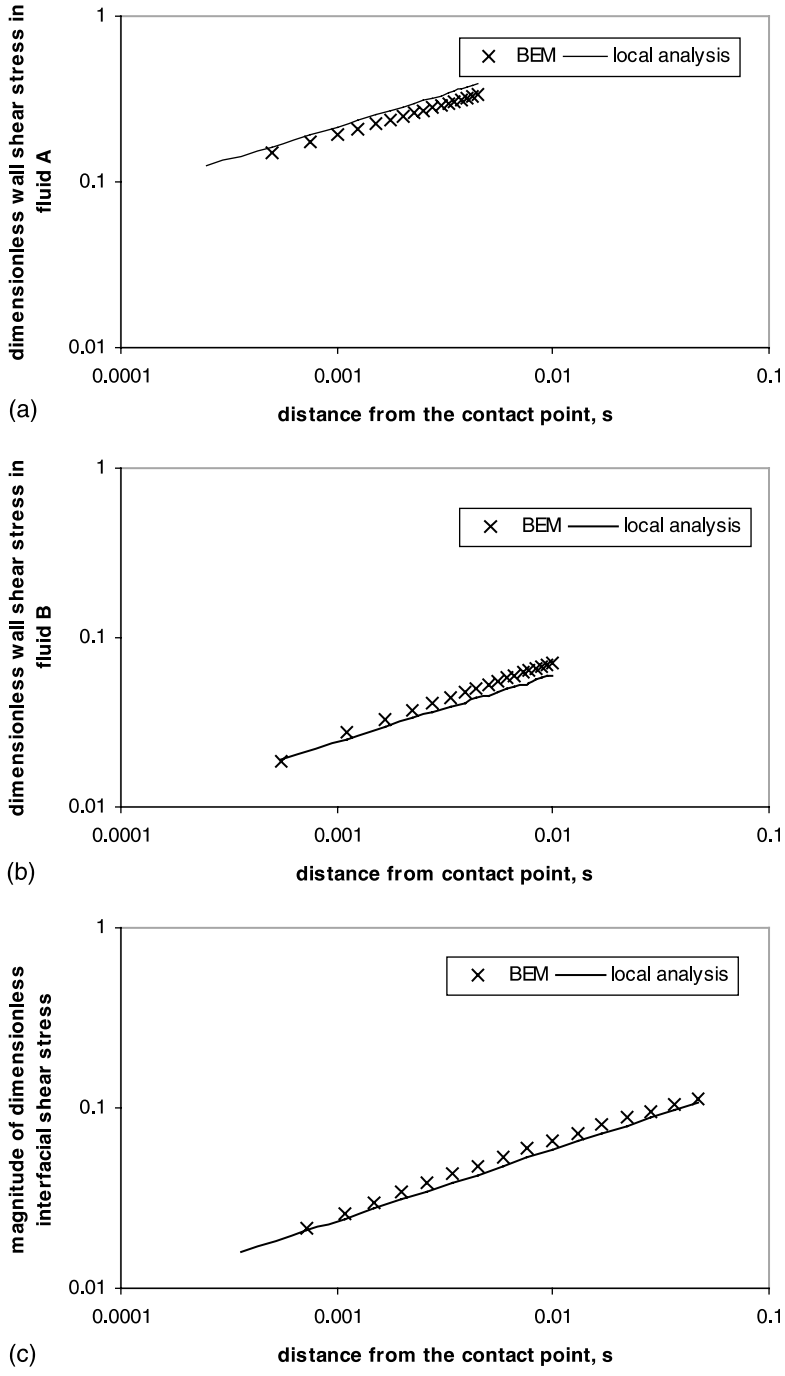

Fig. 20. The variation of the dimensionless shear stress with distance from the contact point, Case II stress approaches zero ($\varepsilon = 0.3$, $\theta = 2\pi/3$, $Bo = 10$, $m = 40$, $\chi = 1$): (a) wall shear stress in fluid A, (b) wall shear stress in fluid B and (c) interfacial shear stress (magnitude).

References

Banerjee, P.K., 1994. The Boundary Element Methods in Engineering, 2nd ed. McGraw-Hill International, London.
Bentwich, M., 1964. Two-phase viscous axial flow in a pipe. Trans. ASME D 86, 669–672.
Bentwich, M., 1976. Two phase axial laminar flow in a pipe with naturally curved interface. Chem. Eng. Sci. 31, 71–76.
Biberg, D., Halvorsen, G., 2000. Wall and interfacial shear stress in pressure driven two-phase laminar stratified pipe flow. Int. J. Multiphase Flow 26, 1645–1673.
Brauner, N., Rovinsky, J., Moalem Maron, D.M., 1996. Analytical solution for laminar–laminar two-phase stratified flow in circular conduits. Chem. Eng. Commun. 141–142, 103–143.
Brauner, N., Moalem Maron, D.M., Rovinsky, J., 1998. A two-fluid model for stratified flows with curved interfaces. Int. J. Multiphase Flow 24, 975–1004.
Brebbia, C.A., 1978. The Boundary Element Method for Engineers. Pentech Press, London.
Davis, A.M.J., Mai, T.Z., 1991. Steady pressure-driven non-Newtonian flow in a partially filled pipe. J. Non-Newtonian Fluid Mech. 41, 81–100.
El-Zafrany, A., 1993. Techniques of the Boundary Element Method. Ellis Horwood Limited, West Sussex.
Gemmell, A.R., Epstein, N., 1962. Numerical analysis of stratified laminar flow of two immiscible Newtonian liquids in a circular pipe. Can. J. Chem. Eng. 40, 215–224.
Gorelik, D., Brauner, N., 1999. The interface configuration in two-phase stratified pipe flows. Int. J. Multiphase Flow 25, 977–1007.
Hall, A.R.W., 1992. Multiphase flow of oil, water and gas in horizontal pipes. Ph.D. Thesis, University of London.
Hall, A.R.W., Hewitt, G.F., 1993. Application of two-fluid analysis to laminar stratified oil-water flows. Int. J. Multiphase Flow 19, 711–717.
Kurban, A.P.A., 1997. Stratified liquid–liquid flow. Ph.D. Thesis, University of London.
Moalem Maron, D.M., Brauner, N., Rovinsky, J., 1995. Analytical prediction of the interface curvature and its effects on stratified two-phase flow characteristics. In: Proceedings of International Symposium on Two-phase Flow Modeling and Experimentation 3, 163–170.
Ng, T.S., Lawrence, C.J., Hewitt, G.F., 1999a. Integral and local flow property calculations of stratified two-phase flow using a boundary integral method. Multiphase Flow Systems Report WASP/47 MPS/123, Imperial College, London.
Ng, T.S., Lawrence, C.J., Hewitt, G.F., 1999b. A detailed analysis of smooth stratified laminar flow in a pipe. In: Proceedings of the 37th European Two-Phase Flow Group Meeting, London, 28–30 September, 1999.
Ng, T.S., Lawrence, C.J., Hewitt, G.F., 2001. Interface shapes for two-phase laminar stratified flow in a circular pipe. Int. J. Multiphase Flow 27, 1301–1311.
Packham, B.A., Shail, R., 1971. Stratified laminar flow of two immiscible fluids. Proc. Camb. Phil. Soc. 69, 443–448.
Pozrikidis, C., 1992. Boundary Integral and Singularity Methods for Linearlised Viscous Flow. Cambridge University Press, Cambridge.
Ranger, K.B., Davis, A.M.J., 1979. Steady pressure driven two-phase stratified laminar flow through a pipe. Can. J. Chem. Eng. 57, 688–691.
Rusell, T.W.F., Charles, M.E., 1959. The effect of the less viscous liquid in the laminar flow of two immiscible liquids. Can. J. Chem. Eng. 27, 18–34.
Stakgold, I., 1979. Green's Functions and Boundary Value Problems. Wiley-Interscience, New York.
Yu, H.S., Sparrow, E.M., 1967. Stratified laminar flow in ducts of arbitrary shape. AIChE J. 13, 10–16.